1991MNRAS.253..686C

Mon. Not. R. astr. Soc. (1991) **253**, 686–702

A spectroscopic survey of faint compact objects

Matthew Colless,[1] Richard S. Ellis,[2] Keith Taylor[3] and Graham Shaw[2]

[1] *Institute of Astronomy, The Observatories, Madingley Road, Cambridge CB3 0HA*
[2] *Physics Department, University of Durham, South Road, Durham DH1 3LE*
[3] *Anglo-Australian Observatory, PO Box 296, Epping, NSW 2121, Australia*

Accepted 1991 July 31. Received 1991 July 31; in original form 1991 May 9

SUMMARY

We present results from a low-resolution (73 Å) spectroscopic survey of faint compact objects conducted with the Low Dispersion Survey Spectrograph at the Anglo-Australian Telescope. The sample is a random subset of all compact sources with $22.5 \leqslant b_J \leqslant 23.5$ in three high-latitude fields. Additional data on compact sources with $21 \leqslant b_J \leqslant 22.5$ have been selected from the higher resolution (13 Å) survey previously published by Colless *et al.* (1990), and a subset of these brighter objects has been studied at both dispersions. The new fainter survey was motivated by the possibility of discovering rare, but potentially important, populations of hitherto unidentified compact sources and establishing limits on their contributions to the source counts. Low-dispersion spectra have been secured for 117 new sources, of which spectroscopic identifications are possible for 67. Incompleteness arises primarily because only certain types of object have spectral features recognizable at this low dispersion. The bulk of the identified sources are intermediate- and late-type stars but a few galaxies and QSOs are also found. Completeness is a strong function of optical colour however, permitting us to derive important new constraints on the abundance of three populations at faint magnitudes as follows. (1) We demonstrate that our survey is sensitive to the presence of typical QSOs with broad emission features, and obtain limits on the surface density of QSOs at fainter magnitudes than previously possible. Our estimates support a flattening of the count–magnitude relation beyond $b_J = 20$, as indicated by earlier work at brighter magnitudes. This result is especially significant since our sample is selected only by apparent magnitude, and is thus more inclusive than previous studies which have relied on additional selection criteria such as colour or variability. (2) For faint Galactic stars, we find a colour–magnitude distribution that is consistent with models invoking an intermediate population II thick disc. More complete and extensive data would provide numerical constraints on such models. (3) Finally, we investigate whether locally rare populations may make significant contributions to the very faint ($B \sim 27$) source counts. The paucity of very *blue* compact sources in the LDSS survey suggests the abundance of such objects at fainter limits arises via a gradual increase in the star formation rates in the galaxy population, rather than via a Euclidean increase due to a compact local population or a sudden onset with apparent magnitude of very distant sources. The absence of *red* objects in the very faint colour distribution, together with the dominant population of Galactic stars in the LDSS sample, limits any significant contribution from dwarf stellar systems such as intergalactic globular clusters and dE galaxies.

1 INTRODUCTION

The value of statistically complete spectroscopic surveys has become increasingly apparent in recent years, especially at faint limiting magnitudes where multiple object techniques have accelerated progress in studies of faint galaxies, QSOs and Galactic stars (*cf.* Ellis & Parry 1988). The targets for such surveys usually represent a select subset of the entire population. In studies of galaxies, stellar objects are eliminated by selecting only extended images; in studies of QSOs,

© Royal Astronomical Society • Provided by the NASA Astrophysics Data System

1991MNRAS.253..686C

variability, proper motions and broad-band colours have been employed to select candidates from among the much larger number of stars. The question frequently arises as to whether such pre-selection techniques bias the results of such surveys. How many compact galaxies are misclassified as stars? Are the QSO counts derived from ultraviolet excess criteria representative of the overall QSO population? A further question concerns the identification of entirely new classes of objects. At faint magnitudes, types of object with very low space densities may finally emerge as an abundant proportion of the total population because of the Euclidean slope of their source counts.

Ultimately, such questions can only be answered by spectroscopically surveying *all* objects, regardless of classification, colour or other properties, down to some fixed limit of magnitude or flux. In a pioneering study, Tritton & Morton (1984) and Morton, Krug & Tritton (1985) systematically obtained $B-V$ colours and spectroscopic classifications for nearly all of the approximately 750 objects brighter than $B=20$ in a 0.31-deg^{-2} area. At a limit 2.5 magnitudes fainter, Colless *et al.* (1990, hereafter Paper I) used the newly commissioned *Low Dispersion Survey Spectrograph* (LDSS) at the 3.9-m Anglo-Australian Telescope (AAT) to classify 120 sources out of a sample of 149 randomly chosen in three high-latitude fields with $21 \leqslant b_J \leqslant 22.5$ ($b_J \equiv$ Kodak IIIa-J + Schott GG385). The incompleteness of 19 per cent arises from the difficulty of securing reliable spectral identifications at these faint limits. Both Morton *et al.* and Paper I found that the ratio of stars to galaxies, as determined from the appearance of images on deep photographic plates, was remarkably similar to that derived from the spectroscopic identifications, although for individual objects the two classification schemes occasionally disagreed.

Paper I was primarily concerned with properties of the *galaxies* to $b_J=22.5$, which formed 73 per cent of the identified population. We now turn to discussing the other objects in the catalogue of Paper I. Since the original survey contained a minority of stars and unidentified sources (33 and 29 respectively), we have carried out in parallel a second deeper survey of *compact* objects reaching one magnitude fainter to $b_J=23.5$. This survey was also performed with LDSS, but using a lower dispersion grism than that used in Paper I. Here, we combine data from the two surveys across $21 \leqslant b_J \leqslant 23.5$ to address the question posed above, and in particular to investigate previously undiscovered populations of faint objects.

A plan of the paper follows. In Section 2 we discuss the selection criteria we have adopted and how, in particular, we have determined a reliable compactness criterion. In Section 3 we briefly review the observational strategy; many of the details are similar to those described in Paper I. We present our spectroscopic catalogue in Section 4 and discuss the various results arising from the number–magnitude relation of faint QSOs (Section 5), and the colour–magnitude distribution of faint stars (Section 6). Finally, in Section 7 we discuss the upper limits we are able to place on previously undiscovered objects of various kinds. We summarize our main results in Section 8.

2 THE SURVEY SAMPLE

The major progress in spectroscopic surveys since the paper by Morton *et al.* (1985) has been the development of techniques for multiobject spectroscopy. Morton *et al.* used a Schmidt objective prism for the bulk of their spectroscopic classification work, resorting to 4-m telescope slit spectroscopy for those objects whose nature remained uncertain.

The Low Dispersion Survey Spectograph (LDSS) described in Paper I and based on the optical design of Wynne & Worswick (1988) was built to cover *both* aspects of Morton *et al.*'s strategy. By using multislit masks, LDSS eliminates the overlapping dispersed sky inherent in slitless data but retains a sufficiently wide field to maintain a significant multiplex gain for faint survey work. Using a 870 Å mm^{-1} grism (hereafter 'low dispersion'), between 50 and 100 objects can be simultaneously observed to $B \approx 23$–24. Thus the instrument offers a parallel to Morton *et al.*'s objective prism survey, but to a limit 3–4 magnitudes fainter. Using the 170 Å mm^{-1} grism (hereafter 'intermediate dispersion'), 20–40 objects can be simultaneously observed, and the resolution is such that weak absorption features are recognized in the vast majority of faint targets.

During our early observing campaigns on the AAT, two surveys were executed in parallel: an intermediate-dispersion survey of all objects (regardless of appearance) with $21 \leqslant b_J \leqslant 22.5$, and a low-dispersion survey of compact objects with $22.5 \leqslant b_J \leqslant 23.5$. The choice of magnitude limits was dictated both by the surface density of objects required to make efficient use of the instrument and the signal/noise provided in 3–5 hr integrations. Since the same high-latitude fields were studied in both surveys, a random subset of the compact objects in the first survey were additionally surveyed at low dispersion in the second survey in order to provide some intercalibration between the rather different dispersions.

The selection of all survey samples was done from COSMOS measuring machine photometry and image classifications of deep AAT prime focus b_J, r_F (IIIa-F + RG630) and U (IIIa-J + UG1) plates of two equatorial fields at 10^h44^m ($l=248°$, $b=49°$) and 13^h41^m ($l=330°$, $b=60°$) (see Table 1). The details of the COSMOS measurements and CCD calibrations are described by Jones *et al.* (1991), and independent checks on the photometric precision were discussed in Paper I. The relative magnitudes measured by COSMOS are isophotal and the slightly different isophotal thresholds adopted for the two fields (see Table 1) introduces a systematic error of around 0.1 mag in the faintest uncalibrated photometry. To overcome this, each field was independently calibrated using 'total' CCD magnitudes for faint sequences of stars and galaxies. Jones *et al.* (1991) estimate that the absolute photometry is accurate to better than 0.1 mag at the bright end of the survey range ($b_J=21$, $r_F<20.5$), with the errors increasing to ~ 0.2 mag at the faint limit ($b_J=23.5$, $r_F<21.5$). The rms photometric error for individual objects increases from ± 0.11 to ± 0.29 mag in b_J and from ± 0.18 to ± 0.37 mag in r_F. Note that there are small ($\leqslant 0.06$ mag) variations in the sample magnitude ranges because of small refinements in the photometric zero-points made after the objects were selected.

Two LDSS survey zones were observed in each field (see Table 2). The primary sample of compact objects, those with $22.5 \leqslant b_J \leqslant 23.5$, were selected to form a fair one-in-two sample of compact objects in this magnitude range in these zones (the selected objects form a fair sample at the 81 per cent confidence level under a Kolmogorov–Smirnov test). A further sample of compact objects with $21 \leqslant b_J \leqslant 22.5$

© Royal Astronomical Society • Provided by the NASA Astrophysics Data System

1991MNRAS.253..686C

Table 1. Summary of the photographic photometry.

Field	Band	AAT plates	Seeing (arcsec)	Isophote (mag arcsec^{-2})	Survey range (mag)
10hr	b_J	J1834	1.7	26.44	$20.98 \leq b_J \leq 23.48$
	r_F	F1835	1.8	24.61	
	U	U2206	2.0	25.09	
13hr	b_J	J1836	1.8	26.52	$20.94 \leq b_J \leq 23.44$
	r_F	F1837	2.3	24.82	$(20.00 \leq b_J \leq 23.60$
	U	U2208	2.3	24.88	in zone 13.1)

Table 2. The survey observations.

Survey zone	α (1950)	δ (1950)	Obsvn dates	Detector	Exposure time (s)	Area (deg^2)
10.2	10 43 55.4	+00 05 33	18/3/88	IPCS	15000	0.0330
10.4	10 43 51.4	−00 06 41	20/3/88	IPCS	13500	0.0330
13.1	13 40 32.0	+00 13 22	1–2/6/86	CCD	14500	0.0078
13.2	13 41 57.3	+00 06 25	18/3/88	IPCS	12000	0.0330

present in the intermediate dispersion survey (Paper I) was also included as described above. These calibration objects form a fair one-in-five sample at the 14 per cent confidence level (K–S test). In the first survey zone attempted (13.1), the compact objects were selected from a slightly wider magnitude range, $20 \leqslant b_J \leqslant 23.6$. In total, 128 targets were examined in the four zones of the survey.

We selected objects from the b_J sample regardless of whether they were seen on plates in other passbands. Whilst this increases the likelihood of observing spurious objects, it introduces no colour biases that would otherwise enter close to the respective plate limits. For $b_J \approx 21$, over 95 per cent of objects are matched on the corresponding r_F plate and over 90 per cent on the corresponding U plate, but at $b_J \approx 23.5$ the matched fractions drop to 75 per cent (r_F) and 40 per cent (U).

Since part of the motivation for including all objects in Paper I was the uncertainty in distinguishing stars from galaxies at $b_J = 22.5$, the selection of a set of compact objects to $b_J = 23.5$ evidently requires some care. A major difficulty is that galaxies considerably outnumber stars at faint limits. Ideally, the fraction of stars that any selection procedure omits must be small to ensure the sample is near-complete, while to be *effective* it must include as small a fraction of galaxies in the sample as possible. Since a major motivation of our study is the spectroscopic determination of the number of extragalactic objects that lie otherwise undiscovered in the compact object category, it is safer to include marginals rather than reject them, even though this may reduce the size of the useful statistical samples per night of telescope time.

Various techniques have been used to separate stars from galaxies at faint limits. Generally speaking, each method becomes less effective with increasing apparent magnitude. Jones *et al.* found that the scattergram of $\log[(I_{\rm peak} - I_{\rm sky})/I_{\rm sky}]$ versus b_J [see their fig. 1(b)] is effective at magnitudes sufficiently faint that the peak surface brightness ($I_{\rm peak}$) of stars is not saturated. Their separating locus was determined using a master set of 800 visually classified images evenly distributed in magnitude and position on each plate. They applied this star–galaxy separation procedure to the b_J, r_F and U plates of each field independently. Good agreement was found between the classifications in the different passbands; in cases of disagreement the b_J classification was adopted, since the b_J plates were taken in slightly better seeing (see Table 1). Jones *et al.* found that this procedure gave reliable star–galaxy separation to $b_J \approx 22$; fainter than this the star and galaxy locii, as determined from visual typing, begin to overlap significantly on the scattergram.

Although such a procedure does not reliably classify *individual* stars and galaxies fainter than $b_J \approx 22$, the distance from an extrapolation of the separation locus in the $\log[(I_{\rm peak} - I_{\rm sky})/I_{\rm sky})]$ versus b_J diagram might be used as an 'image compactness criterion' to select a *statistical* sample with minimal confusion of stars and galaxies. Fortunately, a direct check on their star–galaxy separation for the range $21 \leqslant b_J \leqslant 22.5$ can be made from the spectroscopic classifications of Paper I. In this magnitude range, out of 33 objects identified spectroscopically as stars four were misclassified as galaxies, implying an *incompleteness* in stars in the compact object class of only 12 per cent. This relatively low level of incompleteness is obtained at the expense of significant contamination of the sample by galaxies. For 43 images classed as stars, 14 objects were found spectroscopically to be galaxies, implying a *contamination* of the compact object class of 33 per cent. The high contamination rate is not due to any bias in the star–galaxy separation procedure, as the fractions of stars and galaxies misclassified are in fact very similar (13 and 16 per cent respectively). It is rather a consequence of the high ratio (about 4:1) of galaxies to stars at these magnitudes.

In the magnitude range $22.5 \leqslant b_J \leqslant 23.5$ we cannot make a direct spectroscopic check on the star–galaxy separation. This is a primary motivation of our survey. In this sense, some extrapolation of the separating locus tested at brighter magnitudes is unavoidable to make progress. However we *can* estimate the *stability* of our primary criterion by considering the effects of the increasing noise in the image parameters at fainter magnitudes, and the increasing convergence of star and galaxy image properties. We attempt to do this by comparing the Jones *et al.* classification procedure with another measure of image compactness derived from the log(isophotal area) versus b_J diagram. These two compactness measures are physically correlated, but, in the limit of noisy image parameters, statistically nearly independent.

As noted above, the Jones *et al.* classifier yields approximately equal fractions of misclassified stars and galaxies for $21 \leqslant b_J \leqslant 22.5$. We therefore adopt a separating locus in the log(area) versus b_J scattergram which leads to a similar balance. Figs 1(a) and (b) show log(isophotal area) versus b_J scattergrams for objects in the two fields using the Jones *et al.* classifications and the adopted locii. Now, over the range $21 \leqslant b_J \leqslant 22.5$ where a spectroscopic check is possible, the fraction of both stars and galaxies classified *differently* by the two schemes is 11 per cent. If the log(area) method misclassifies roughly the same (and equal) fractions of stars and galaxies as the Jones *et al.* procedure, this difference implies that the sample of compact objects is only 6 per cent incomplete in stars and has 19 per cent contamination by galaxies. These estimates are significantly less than the estimates for this magnitude range obtained from the spectroscopic check above and suggest our two classification methods make correlated errors and so are not completely independent. Further progress might be possible with independent high-quality imaging data, but of course over such a panoramic field this is difficult with CCD detectors.

© Royal Astronomical Society • Provided by the NASA Astrophysics Data System

1991MNRAS.253..686C

In extending this discussion to the full magnitude range of our new spectroscopic survey, we can only derive completeness and contamination estimates on the assumption that the two classifiers disagree by the same fraction of the total error as is the case for the magnitude range tested above. For $21 \leqslant b_J \leqslant 23.5$ the classifiers disagree at the 15 per cent level, implying that the full survey sample is 8 per cent incomplete in stars and has 39 per cent contamination by galaxies. Adopting the same fractions as in the brighter magnitude range, we would expect the true incompleteness to be 16 per cent and the true contamination to be 68 per cent. Although crude, we believe these are the best estimates possible in the absence of further information.

A contamination rate in our compact object class of 40–70 per cent by galaxies might at first seem disappointing, since it implies we have to look at 1–2 galaxies for every genuine compact object in the sample. However if *no* compactness criterion had been applied, the overhead would be ~7 galaxies for each compact object, leading to a *tripling* of the observing time necessary to acquire a stellar sample of the same size. Given our desire to maintain a high level of completeness, this is a reasonable compromise.

3 OBSERVATIONS AND REDUCTIONS

The observations were carried out with the Low Dispersion Survey Spectrograph (LDSS) on the AAT during observing runs in 1986 May and 1988 March. In 1986 we used a RCA CCD detector, giving an effective field of view of 6.7×4.2 arcmin. One survey zone of this size in the 13-hr field (13.1) was observed with this configuration. In 1988 we changed to the Image Photon Counting System (IPCS), which provides an effective circular field of 12.3 arcmin in diameter. Three zones of this size in both the 10-hr and 13-hr fields (10.2, 10.4 and 13.2) were observed. The details are summarized in Table 2.

Total integration times for all four zones were between 12 000 and 15 000 s. Although the RCA CCD is ~5 times as efficient as the IPCS, so that the data in zone 13.1 are at higher S/N than the rest, we discovered that the CCD suffers from a relatively high rate of cosmic ray events that are hard to distinguish from spectral features. Because of this, the IPCS was the preferred detector for subsequent runs. Its lower detection efficiency is compensated by its fourfold increase in field area and the proportionally smaller amount of time spent on field acquisition. The low-dispersion (870 Å mm^{-1}) grism used in this survey gives a FWHM resolution (measured from calibration lamp lines) of 73 Å (2.8 pixels) for both detectors (each of which had 30-μm pixels in the spectral dimension). The effective spectral range is 3700–7500 Å.

The reduction procedures applied to the IPCS data are more or less identical to those described in Paper I. Briefly, the raw image is first corrected for spatial distortions introduced by the optics and (more importantly) the magnetic focusing of the IPCS. The correction transformation is determined by imaging a white light source through a mask with a regular grid of holes at known positions. This transformation is used to resample the images of both the wavelength calibration lamps and the targets. Plate 1 shows the LDSS spectral image obtained for one of the fields after co-adding distortion-corrected IPCS frames with a total integration time of 12 000 s.

Calibration images are observed through the same mask as the targets, enabling a wavelength transformation to be determined for each of the slits in the mask. For the helium lamps used, second-order polynomial fits to nine lines spanning 3888 to 7281 Å gave rms errors of $\leqslant 6$ Å (i.e. $\leqslant 0.1$ resolution element). Each slit spectrum is then sky-subtracted by fitting a low-order polynomial to the undispersed profile (omitting the interval containing the object) and subtracting the fitted slit profile (appropriately normalized) from each column of the image. The object spectrum is extracted in a near-optimal fashion, weighting the rows of its spatial cross-section by the best-fitting Gaussian. Once extracted the spectrum is wavelength-calibrated and put on a relative flux scale. The flux scale was determined for the 1988 IPCS data from a comparison of long slit and slitless observations of the Oke (1974) flux standard L970-30. For the 1986 CCD data the flux scale is based on the Oke standard GD190.

4 THE SURVEY CATALOGUE

A total of 128 target objects, selected according to the prescription of Section 2, were observed over the four zones of the survey. 11 objects were not detected spectroscopically, even when the slit profile was summed over the entire spectral range. Examination of the plates revealed that eight of these 'objects' represent spurious COSMOS detections; nearly all are in the 10-hr field. Three are detected in r_F and their non-detection could represent errors in astrometry or mask manufacture, or the effects of inaccurate acquisition near the edges of the LDSS field of view. Regardless of the precise cause, the deletion of these 11 objects from further consideration will not affect our statistical analyses.

Table 3 presents the survey catalogue which contains the position, b_J magnitude, and $b_J - r_F$ and $U - b_J$ colours for the 117 detected objects. For each object, the spectrum was examined and given one of the following spectral identifications (SIDs): (i) an approximate stellar type for M stars; (ii) *star*, for stars of earlier spectral types, usually recognized by the Mg I *b*-band; (iii) *qso*, for QSOs; (iv) *elg*, for emission line galaxies with two or more identified lines; (v) *gal*, for galaxies showing the Ca $H+K$ break at 4000 Å; (vi) *em*?, for spectra showing one or more unidentified emission features; and (vii) ???, for unidentifiable spectra (whether due to poor signal/noise or lack of spectral features).

A significant proportion of the sample are M stars which are readily recognized at low dispersion because of their prominent molecular absorption bands. In order to obtain an approximate spectral type for these, all spectra were cross-correlated against a set of M star template spectra (comprising M0V, M1V, M3III, M5III and M5V spectral types) drawn from the library of Jacoby, Hunter & Christian (1984). The normalized height of the highest peak in the cross-correlation function (CCF) is indicative of the degree of match between the object spectrum and the template. A *credibility index* for spectral matches was constructed by noting that for genuine stars the best match (the highest CCF peak) occurs when there is no relative wavelength shift between the object and template spectra (at our low resolution all stars effectively have zero velocities). The credibility index for a particular template is defined at a given CCF peak height to be the fraction of best matches that have offsets of less than one resolution element.

© Royal Astronomical Society • Provided by the NASA Astrophysics Data System

1991MNRAS.253..686C

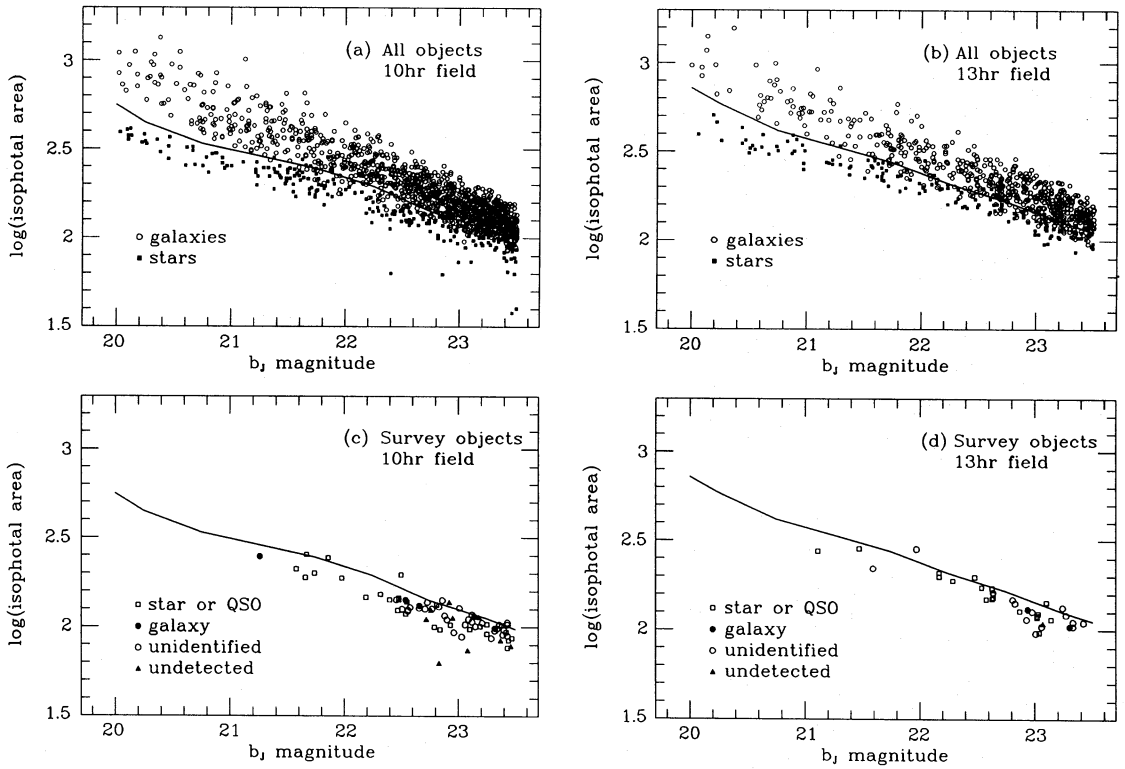

Figure 1. (a), (b) The distribution of log(isophotal area) with b_J magnitude for the objects classified as stars and galaxies in the two survey fields. The solid line is the selection criterion that results in equal fractions of stars and galaxies being misclassified. (c), (d) The distribution of log(isophotal area) with b_J for the objects in the survey, showing their spectroscopic identifications. The solid lines are the same as those in (a) and (b).

Table 3. The survey catalogue.

ID	α (1950)	δ	b_J	b_J-r_F	$U-b_J$	z	SID	Comments
10.2.01	10 44 06.60	+00 08 13.5	21.58	0.51	-0.22	1.607	qso	CIV,CIII,MgII
10.2.02	10 43 45.52	+00 07 51.9	21.74	2.19	—	—	M5V	
10.2.03	10 44 04.87	+00 06 55.2	21.98	2.16	—	—	M5V	
10.2.04	10 43 53.08	+00 03 54.7	22.19	2.41	—	—	M5V	
10.2.05	10 43 47.59	+00 09 19.5	22.40	2.23	—	—	M5V	
10.2.06	10 44 00.99	+00 07 28.9	22.46	1.49	—	—	???	
10.2.07	10 43 49.07	+00 02 33.8	22.48	1.98	—	—	M0V	
10.2.08	10 44 07.30	+00 01 00.6	22.50	2.28	—	—	M0V	
10.2.09	10 43 57.65	+00 02 16.0	22.55	0.50	-0.81	2.014	qso	NV,CIV,HeII,CIII
10.2.10	10 43 41.84	+00 01 10.8	22.58	0.89	-0.64	—	em?	7250Å
10.2.11	10 43 37.21	+00 06 01.4	22.66	1.90	—	0.030	elg	[OII],Hα,G,MgIb
10.2.14	10 43 44.51	+00 06 58.5	22.79	2.54	—	—	M5V	
10.2.15	10 44 01.23	+00 05 38.9	22.81	2.37	—	—	M5V	
10.2.16	10 43 54.91	+00 09 44.5	22.83	1.52	-0.02	—	em?	6950Å
10.2.18	10 43 35.72	+00 06 45.4	22.84	2.42	—	—	M5V	
10.2.19	10 44 09.01	+00 05 10.8	22.86	1.53	—	—	em?	4000Å
10.2.20	10 43 41.91	+00 08 58.0	22.88	1.23	—	—	???	
10.2.21	10 43 50.29	+00 00 18.5	22.90	1.28	-0.02	—	???	
10.2.22	10 44 05.32	+00 03 34.9	22.93	2.54	—	—	M5V	
10.2.23	10 44 18.74	+00 04 44.2	23.06	1.56	-0.75	—	em?	6600Å
10.2.25	10 43 40.89	+00 10 13.1	23.09	0.64	—	—	???	
10.2.26	10 43 41.13	+00 07 33.4	23.10	2.32	—	—	M0V	
10.2.27	10 43 37.72	+00 05 42.2	23.14	—	-0.19	0.134	gal	CaH+K,MgIb
10.2.29	10 43 58.95	+00 10 32.0	23.25	2.62	—	—	M5V	
10.2.30	10 43 44.52	+00 08 23.5	23.36	2.54	—	—	???	
10.2.31	10 43 43.84	+00 04 33.5	23.39	1.11	—	—	???	
10.2.32	10 44 04.67	+00 08 55.8	23.40	1.22	—	—	???	
10.2.33	10 43 56.99	+00 10 13.5	23.43	1.84	—	—	???	
10.2.34	10 43 35.62	+00 02 12.4	23.44	—	-0.99	—	M5V	
10.2.35	10 43 34.50	+00 03 54.3	23.47	2.15	—	—	M5III	
10.4.01	10 43 45.68	−00 02 35.8	21.26	1.38	-0.53	0.320	elg	[OII],[OIII]
10.4.02	10 43 55.30	−00 09 08.4	21.66	1.27	-0.07	—	M5V	
10.4.03	10 43 46.82	−00 11 08.6	21.67	2.32	—	—	M5V	
10.4.04	10 43 56.76	−00 11 28.3	21.86	1.96	—	—	M0V	
10.4.05	10 43 47.34	−00 02 17.8	22.32	2.11	—	—	M5V	
10.4.06	10 43 56.11	−00 10 46.8	22.47	1.57	—	—	M0V	
10.4.07	10 43 54.47	−00 08 11.1	22.48	2.06	—	—	star	
10.4.08	10 44 15.17	−00 07 34.9	22.51	—	—	—	???	
10.4.09	10 43 56.30	−00 07 41.6	22.54	1.76	—	0.168	gal	CaH+K
10.4.10	10 43 33.57	−00 09 16.2	22.54	2.24	—	—	M5V	
10.4.11	10 43 34.72	−00 05 37.8	22.56	1.22	0.15	—	???	
10.4.12	10 43 40.98	−00 01 11.1	22.56	2.00	—	—	???	
10.4.13	10 43 40.72	−00 05 17.2	22.66	2.35	—	—	???	
10.4.14	10 43 57.53	−00 10 05.5	22.71	0.98	—	—	???	
10.4.15	10 43 42.26	−00 03 04.3	22.73	0.95	—	—	???	

Table 3 – *continued*

ID	α (1950)	δ	b_J	b_J-r_F	$U-b_J$	z	SID	Comments
10.4.16	10 44 11.37	−00 08 51.0	22.77	1.12	—	—	???	
10.4.19	10 44 05.02	−00 09 46.3	22.96	1.78	-0.17	—	em?	6400Å
10.4.20	10 44 01.39	−00 06 21.7	23.01	1.00	—	—	???	
10.4.21	10 43 46.56	−00 06 09.9	23.03	1.11	-0.37	—	???	
10.4.22	10 44 05.07	−00 07 22.9	23.12	2.28	—	—	???	
10.4.23	10 43 55.65	−00 08 31.4	23.12	1.09	—	—	???	
10.4.24	10 44 10.41	−00 03 04.9	23.15	2.13	—	—	???	
10.4.26	10 44 06.95	−00 02 17.6	23.19	1.93	—	—	M0V	
10.4.27	10 44 12.50	−00 06 59.1	23.21	0.87	—	—	???	
10.4.28	10 43 53.50	−00 04 32.4	23.25	2.31	—	—	M0V	
10.4.29	10 43 41.93	−00 10 07.3	23.29	1.06	-1.58	—	em?	6400Å,6500Å
10.4.30	10 44 08.87	−00 03 35.8	23.32	2.46	—	0.400	gal	[OII],CaH+K
10.4.31	10 43 39.69	−00 10 24.1	23.32	2.11	—	—	???	
10.4.32	10 43 39.57	−00 07 52.5	23.34	1.18	-0.50	—	???	
10.4.34	10 43 40.29	−00 04 51.6	23.38	1.24	—	—	star	
10.4.35	10 44 04.19	−00 09 25.3	23.42	2.32	—	—	M5V	
10.4.36	10 44 10.48	−00 08 13.0	23.43	—	—	—	???	
10.4.37	10 44 08.07	−00 05 50.4	23.43	2.36	—	—	M5V	
10.4.38	10 43 55.35	−00 12 23.8	23.43	1.79	—	—	???	
13.1.01	13 40 37.97	+00 12 09.0	23.44	2.56	—	—	M5V	
13.1.02	13 40 30.97	+00 11 51.7	20.26	0.92	0.13	—	M0V	
13.1.03	13 40 31.48	+00 11 06.8	22.53	1.16	0.86	—	star	
13.1.04	13 40 22.82	+00 12 24.5	22.78	2.16	1.20	—	star	
13.1.05	13 40 29.39	+00 12 40.9	21.54	2.22	1.53	—	M5V	
13.1.06	13 40 26.79	+00 12 54.7	22.43	2.27	—	—	M5V	
13.1.07	13 40 22.30	+00 13 07.3	23.59	2.60	—	—	M5V	
13.1.08	13 40 21.84	+00 13 19.6	21.11	0.39	-0.19	—	star	
13.1.09	13 40 19.98	+00 11 41.4	22.41	0.95	-0.66	—	???	
13.1.10	13 40 40.24	+00 13 29.7	22.82	1.02	0.66	—	???	
13.1.11	13 40 22.93	+00 13 33.8	20.01	0.67	-0.19	—	???	
13.1.12	13 40 31.75	+00 14 11.7	21.54	1.11	0.47	—	???	
13.1.13	13 40 21.37	+00 14 38.8	20.86	0.47	-0.44	—	M5V	
13.1.14	13 40 38.69	+00 14 54.1	23.19	1.88	0.79	—	star	
13.1.15	13 40 38.72	+00 14 41.3	22.53	2.17	—	—	M5V	
13.1.16	13 40 26.82	+00 14 57.2	21.75	0.58	0.12	—	M5III	
13.1.17	13 40 21.52	+00 15 14.7	22.03	2.09	1.95	—	M0V	
13.1.18	13 40 18.84	+00 13 50.0	22.62	1.65	—	—	???	
13.2.01	13 42 15.08	+00 06 48.0	21.11	2.04	1.93	—	M0V	
13.2.02	13 42 13.79	+00 09 14.1	21.47	2.03	1.93	—	M0V	
13.2.03	13 41 41.18	+00 04 11.0	21.59	0.91	-0.11	—	???	
13.2.04	13 41 49.99	+00 01 43.8	21.97	0.71	-0.19	—	???	
13.2.05	13 41 56.23	+00 07 47.0	22.17	2.27	—	—	M5V	
13.2.06	13 41 57.03	+00 08 17.2	22.17	1.04	0.98	—	star	see notes
13.2.07	13 41 34.10	+00 05 21.6	22.29	2.00	—	—	M5III	
13.2.08	13 41 47.40	+00 06 08.0	22.48	2.33	—	—	M5V	

© Royal Astronomical Society • Provided by the NASA Astrophysics Data System

1991MNRAS.253..686C

© Royal Astronomical Society • Provided by the NASA Astrophysics Data System

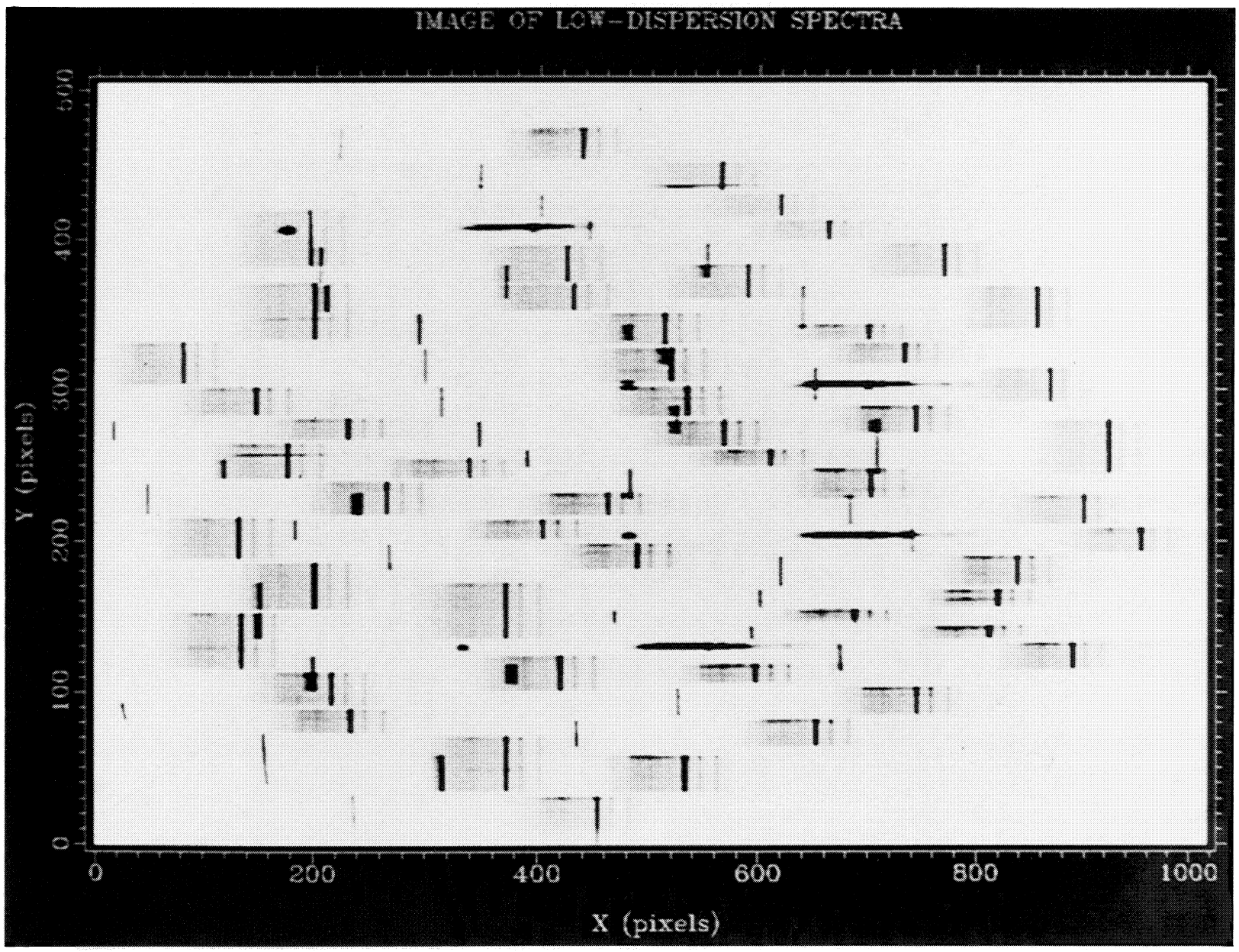

Plate 1. A low-resolution multispectrum image obtained with LDSS. The image has been distortion-corrected within the direct field of view, but distortion is apparent in the corners. Wavelength increases with X pixel number (the bright sky line apparent in every spectrum is [O III] 5577 Å). The four strong, narrow spectra are due to stars in 10-arcsec circular holes which are used as fiducial points during field acquisition. Spectra at the right of the image have corresponding zero-order images, appearing as dark rectangles, at the left. The target object spectra are faintly visible.

1991MNRAS.253..686C

© Royal Astronomical Society • Provided by the NASA Astrophysics Data System

1991MNRAS.253..686C

Table 3 – *continued*

13.2.09	13 41 47.45	+00 08 56.8	22.54	1.38	—	—	M1I	
13.2.10	13 42 00.58	+00 00 27.1	22.58	0.65	0.44	—	M0V	
13.2.11	13 41 54.50	+00 11 43.5	22.63	2.33	—	—	M0V	
13.2.12	13 41 58.67	+00 05 03.1	22.63	2.16	—	—	star	
13.2.13	13 42 12.10	+00 02 06.6	22.64	2.22	—	—	star	
13.2.14	13 41 43.76	+00 10 20.2	22.64	0.63	0.68	—	???	
13.2.15	13 42 00.11	+00 05 53.9	22.64	1.85	—	—	star	
13.2.16	13 41 56.31	+00 01 03.2	22.81	1.11	0.21	—	???	
13.2.17	13 41 45.17	+00 07 28.5	22.83	1.24	0.19	—	???	
13.2.18	13 41 57.30	+00 09 11.8	22.87	2.07	—	—	M5V	
13.2.19	13 41 40.20	+00 04 38.8	22.93	0.62	-0.38	—	???	
13.2.20	13 42 04.89	+00 04 01.7	22.94	1.20	-0.41	0.366	elg	Hβ,[OIII]
13.2.21	13 41 52.24	+00 06 43.1	22.98	0.50	-0.30	—	???	
13.2.22	13 41 53.27	+00 09 50.8	23.01	—	—	—	???	
13.2.23	13 41 38.56	+00 07 53.7	23.02	2.12	—	—	M0V	
13.2.24	13 41 51.65	+00 11 10.8	23.02	2.41	—	—	M5V	
13.2.25	13 41 45.14	+00 02 30.0	23.03	2.41	—	—	M5V	
13.2.26	13 41 52.90	+00 02 51.7	23.04	1.85	—	—	star	
13.2.27	13 42 13.98	+00 10 35.4	23.06	0.81	-0.77	—	???	
13.2.29	13 41 45.72	+00 08 39.0	23.10	2.40	—	—	M5V	
13.2.30	13 41 36.89	+00 05 38.5	23.14	2.21	—	—	M0V	
13.2.31	13 42 01.72	+00 09 29.9	23.24	0.76	—	—	???	
13.2.32	13 42 03.13	+00 05 24.9	23.27	1.37	-0.51	—	???	
13.2.33	13 41 39.21	+00 09 37.0	23.30	—	—	0.444	elg	Hβ,[OIII]
13.2.34	13 42 12.22	+00 07 15.4	23.33	—	—	—	???	
13.2.35	13 41 49.37	+00 10 48.6	23.33	0.91	-0.58	—	???	
13.2.36	13 42 01.22	+00 12 21.6	23.42	—	—	—	???	

Notes. (1) The ID is given in the form *f.z.#*, where *f* is the field R.A., *z* is the zone number, and *#* is the object number within the zone. (2) SID is the spectral ID (see text for details). (3) 13.2.06 is classified *star* from the high-dispersion spectrum of Colless *et al.* (1990).

Fig. 2 shows the credibility index as a function of CCF peak height for each of the M star templates and also for a sky spectrum used as a template. As expected, the index for the sky spectrum remains low at all CCF peak heights, since it only provides a match to the object in the case of poor sky-subtraction. Fig. 2 also shows that the credibility index for the stellar templates begins to rise above the 'noise' level indicated by matches to the sky spectrum for CCF peak heights greater than 0.4. A template was therefore deemed to provide an acceptable match to an object spectrum if both (i) the CCF peak was offset from zero by less than one resolution element and (ii) the CCF peak height was greater than 0.4. Examples of object spectra classified as M stars by this method are shown in Fig. 3 with their best-match template superimposed.

At our low dispersion a significant fraction of the observable wavelength range is obscured by three prominent night sky features ([O III] 5577 Å, Na I 5890 Å and the [O I] 6300 and 6363 Å doublet) and this hampers identifications in cases of poor sky subtraction. For *qso*, *elg* and *gal* SIDs, the redshifts and identified spectral features are also given. The *em*? objects with one or more unidentified features have the wavelengths of the possible emission lines listed in the comments column.

Eight objects in this survey (selected randomly as described in Section 2) were also observed at 13 Å FWHM resolution in the survey of Paper I, providing a valuable check of the low-dispersion SIDs. Of the eight, one object could not be identified at low dispersion (13.2.06) and a further object was classified as *star* from a single Mg *b* feature (10.4.07); both are known to be stars from their high-dispersion spectra. The remaining six were classified as M stars. With this one exception, however, the identifications are supported by the high-dispersion spectra, but one object classified M5V (10.4.05) is identified in Paper I (from a single emission line assumed to be [O II] 3727 Å) as a galaxy at $z=0.237$. The correct identification for this object is not clear, as the high-dispersion spectrum only covers the range

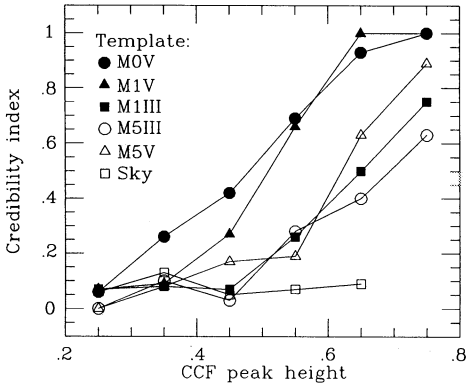

Figure 2. The credibility index of spectral matches (defined in the text) as a function of cross-correlation function peak height for template M star spectra and a sky spectrum.

3700–5400 Å and the emission line is weak. The low-dispersion spectrum *does* have a weak emission feature at the same wavelength, but the spectrum extends to beyond 7000 Å and shows strong absorption features in the red characteristic of M stars. With this one exception, however, the identifications made at low dispersion in the range $21 \leqslant b_J \leqslant 22.5$ are validated by those at higher dispersion.

Of the 117 detected objects in the survey, 58 are identified as stars, four as emission line galaxies, three as galaxies with absorption features, and two as QSOs. Of the 50 objects with identifications, only six have possible emission features. The spectra of the nine extragalactic objects are displayed in Fig. 4, with the features used to identify them marked. The two spectra identified as QSOs (10.2.01 and 10.2.09) are plotted with a superimposed composite QSO spectrum (Francis *et al.* 1991), appropriately redshifted, in order to illustrate the match in the continuum as well as the emission lines.

The overall success rate for spectral identifications in this survey is 57 per cent, significantly lower than the rates of around 80 per cent obtained in the earlier galaxy surveys of Broadhurst, Ellis & Shanks (1988) to $b_J = 21.5$ and of Paper I to $b_J = 22.5$. Fig. 5(a) shows the success rate as a function of apparent magnitude. We see that the completeness in the range $21 \leqslant b_J \leqslant 22.5$ is 83 per cent, comparable to that obtained at intermediate dispersion in Paper I. However, in the fainter range $22.5 \leqslant b_J \leqslant 23.5$ the identification rate drops to 48 per cent. Fig. 5(b) indicates that there is also a strong variation in the identification rate with colour. High completeness is achieved only for objects redder than $b_J - r_F \geqslant 1.8$ (generally M stars with prominent bands) and the bluest objects with $b_J - r_F \leqslant 0.6$ (which often show strong emission lines). The main difficulty we have encountered in this survey is therefore in identifying spectroscopically those objects with intermediate colours fainter than $b_J = 22.5$. Such objects are generally the ones with weaker features for which a higher continuum signal/noise is required.

Fig. 6(a) compares the colour distributions of compact and extended objects in the combined photometric sample from which the survey objects were selected. It shows that to the red of $b_J - r_F \approx 2$ the numbers of stars and galaxies are similar, but that at bluer colours galaxies dominate stars in the ratio 5:1 or more. Fig. 6(b) gives the colour distribution for the survey objects and indicates the spectroscopic identi-

© Royal Astronomical Society • Provided by the NASA Astrophysics Data System

1991MNRAS.253..686C

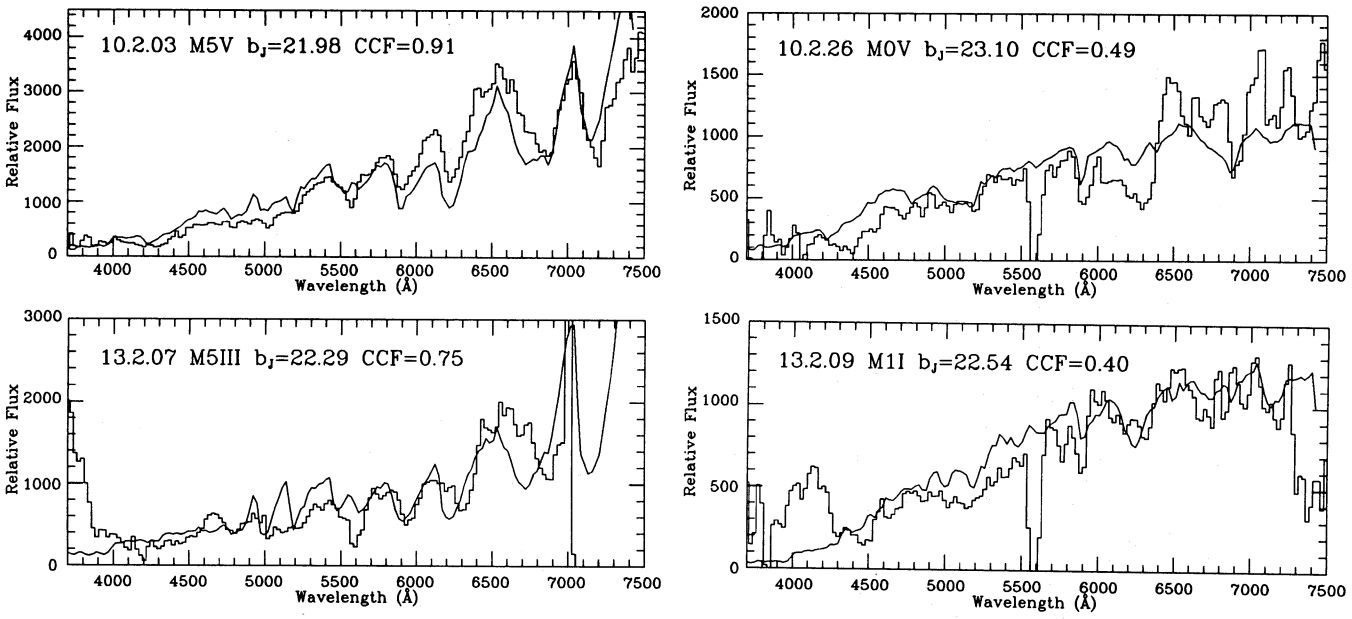

Figure 3. Examples of survey objects classified as M stars using the cross-correlation method. The objects cover a range of magnitudes, spectral types and CCF peak heights. Each object has the spectrum of its best-matching spectral type superimposed. Note that several of the objects show imperfect subtraction of the strong sky lines at 5577, 5892, 6300 and 6363 Å.

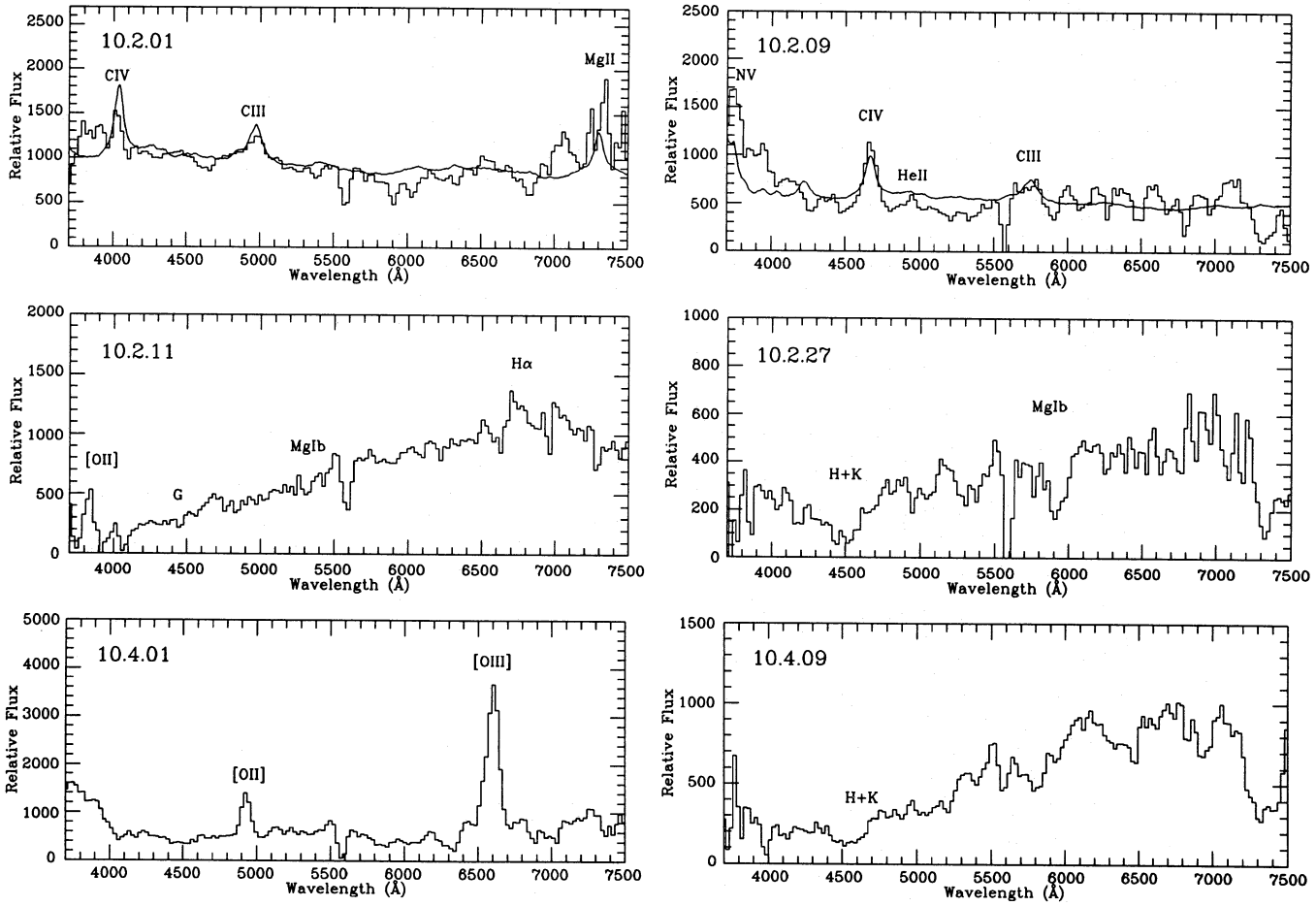

Figure 4. The spectra of the nine extragalactic objects in the survey, showing their identifying features. An appropriately redshifted composite QSO spectrum (Francis *et al.* 1991) is superimposed on the two spectra identified as QSOs. Note that several of the spectra show imperfect subtraction of the strong sky lines at 5577, 5892, 6300 and 6363 Å.

© Royal Astronomical Society • Provided by the NASA Astrophysics Data System

1991MNRAS.253..686C

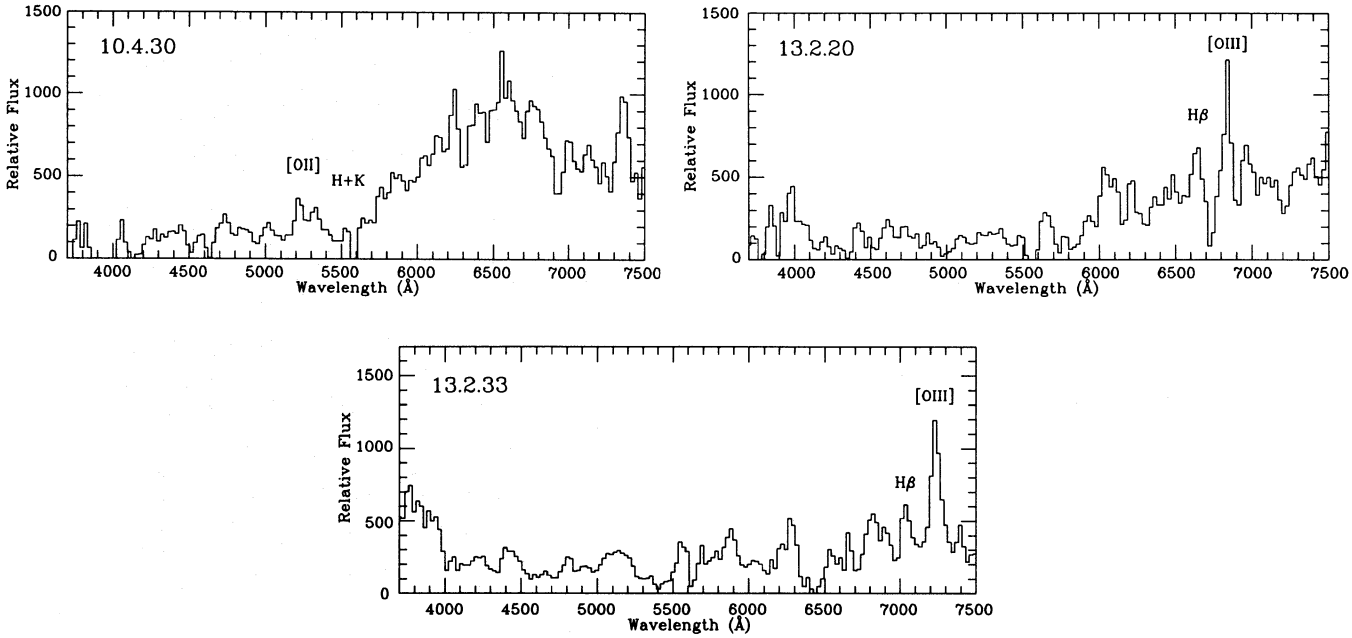

Figure 4 – *continued*

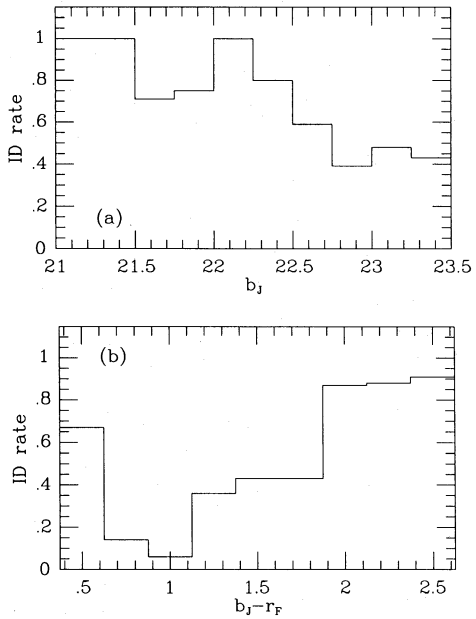

Figure 5. (1) The spectroscopic identification rate as a function of b_J magnitude. (b) The identification rate as a function of $b_J - r_F$ colour.

fications obtained at each colour. The survey objects have the same colour distribution as the compact object sample from which they were drawn, but the spectroscopically identified stars have a much redder distribution. This is in part due to the difficulty of identifying blue stars at the resolution of the survey and in part due to the contamination of the compact object sample by galaxies. Because there are so many more galaxies than stars, the colour distribution for galaxies is negligibly affected by misclassified stars, and must be very similar to that of the extended objects shown in Fig. 6(a). The converse is not true, however, and the arguments of Section 2 led us to conclude that at least 40 per cent of the survey sample are in fact galaxies. This conclusion is consistent with the colour distribution for unidentified objects shown in Fig. 6(b), which peaks at around $b_J - r_F \approx 1.2$, the same colour as the peak of the galaxy distribution.

The actual proportion of contaminating galaxies remains uncertain, but given that just under 50 per cent of our survey are either unidentified objects or identified galaxies, the image classification arguments imply that at least 80 per cent of the unidentified objects are galaxies. This in turn suggests that the survey is at least 85 per cent complete for *bona fide* stars, a success rate consistent with the fact that we failed to identify only one of the seven objects in the overlap sample identified spectroscopically as stars in Paper I.

Despite the serious incompleteness in the colour range $0.6 < b_J - r_F < 1.5$, the homogeneity of our spectra does allow us to place strong limits on the numbers of certain kinds of easily recognizable objects (such as QSOs) and on objects with colours at the extremes of the observed range, where our completeness is highest. The following sections discuss the constraints derived from our survey for these types of object.

5 THE NUMBERS OF FAINT QSOS

This survey represents the faintest systematic survey for QSOs so far performed, with the important bonus that the selection criteria are more inclusive than those used previously (such as selection by colour or variability). Thus whilst the statistical uncertainties in our limits on the faint QSO surface density are large, we can for the first time examine the number of QSOs in a sample of compact objects limited solely by apparent magnitude, enabling us to address the likely completeness of earlier studies. The previous faint limit of $B = 22.5$ was achieved by Koo, Kron & Cudworth

© Royal Astronomical Society • Provided by the NASA Astrophysics Data System

1991MNRAS.253..686C

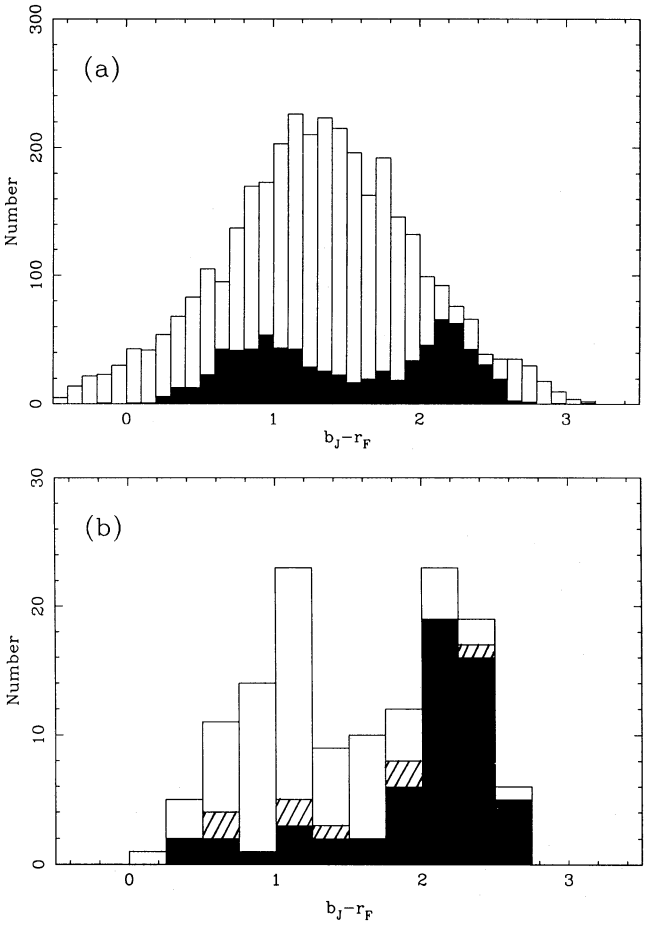

Figure 6. (a) Colour distributions of compact objects (filled histogram) and extended objects (unfilled histogram) with $21 \leqslant b_J \leqslant 23.5$ in the photometric sample from which the survey samples were selected (10- and 13-hr fields combined). (b) Colour distribution of survey objects. The fractions identified as stars are shown by the filled portions, the fractions identified as galaxies or QSOs by the hatched portions, and the unidentified objects by the unfilled portions. (Objects without r_F detections are excluded from both figures.)

(1986) in their survey of compact objects with broad-band colours unlike those of common stars. In principle, our selection criteria would include any putative class of faint QSOs with colours similar to those of ordinary stars.

Only two QSOs are identified in our survey: 10.2.01 at $z = 1.607$ with $b_J = 21.58$ and $U - b_J = -0.22$, and 10.2.09 at $z = 2.014$ with $b_J = 22.55$ and $U - b_J = -0.81$. Both objects have $z < 2.2$ and so would be expected to show an ultraviolet excess (i.e. to be bluer than $U - b_J \approx -0.3$); this is true for 10.2.09, although 10.2.01 is marginal. Assuming $H_0 = 50$ km s^{-1} Mpc^{-1}, and adopting K-corrections from Koo & Kron (1988), the absolute b_J magnitude of 10.2.01 is -24.55 for $q_0 = 0$ (or -23.73 for $q_0 = 0.5$) and of 10.2.09 is -24.18 (or -23.18).

Because the spectral identifications are incomplete, the two identified QSOs give only a *lower* limit to the surface density in the range $21 \leqslant b_J \leqslant 23.5$. A strict (if somewhat crude) *upper* limit is obtained by also counting as QSOs *all* the unidentified objects (i.e. those with SIDs ??? and *em*?, as well as *qso*). Taking into account the total survey area (0.1068 deg^2) and the different sampling rates for objects with $21 \leqslant b_J \leqslant 22.5$ (0.21) and $22.5 \leqslant b_J \leqslant 23.5$ (0.50), we thus obtain lower and upper limits on the surface density of QSOs with $21 \leqslant b_J \leqslant 23.5$ of 64 deg^{-2} and 1100 deg^{-2}. The lower limit is subject to large statistical uncertainties and the upper limit is a considerable overestimate since, as discussed above, the bulk of the unidentified objects are likely to be normal galaxies.

We can, however, make a stronger statement on surface density limits by considering the detectability of QSOs in this survey. The strong, easily recognizable, emission lines of a 'typical' QSO [represented by the composite spectrum constructed by Francis *et al.* (1991)] suggest that most QSOs ought to be recognized unless their features are redshifted outside our wavelength range. We can make the test more quantitative by estimating the detectability of the composite QSO spectrum, as a function of its redshift, for each unidentified spectrum in the LDSS survey. To make this estimate we assume that the detectability of any particular QSO line is directly related to the S/N ratio in the line. We use the relation $S/N_{\rm line} \approx \frac{1}{2}(1+z)^{1/2}\sigma^{-1/2}W_\lambda S/N_{\rm cont}$, where σ is the velocity dispersion of the line profile, W_λ is the rest-frame equivalent width of the line, and $S/N_{\rm cont}$ is the continuum S/N ratio about the redshifted wavelength of the line *in the chosen LDSS spectrum.* The approximate dispersions and equivalent widths of common QSO lines were measured from the Francis *et al.* composite spectrum, while the continuum S/N as a function of wavelength was estimated directly from the LDSS spectrum. By applying this technique to all the unidentified spectra in our survey, we can place a much firmer limit on the surface density of QSOs with spectra similar to that of the composite.

For the two QSOs identified in the survey, we find in 10.2.01 that the detected lines C IV, C III and Mg II have $S/N_{\rm line}$ of 11, 20 and 6.7 respectively, while in 10.2.09 the detected lines N V, C IV and C III have $S/N_{\rm line}$ of 4.6, 7.3 and 3.6. However we would also have expected to detect the unseen Si IV + O IV feature in 10.2.09 with $S/N_{\rm line}$ of 4.0. On the basis of these two examples, it would appear that a QSO will be identified if at least one emission line has $S/N_{\rm line} > 6$ and at least one other, confirming, line has $S/N_{\rm line} > 4$. That is, to claim an identification we demand one unambiguous detection of a line confirmed by at least one other reasonable detection. Fig. 7 then shows the fraction of the unidentified spectra in which a typical QSO would have been detected, if present, as a function of redshift. Note the 'hole' of zero detection probability as Hβ moves out of the spectral range at $z \approx 0.5$ and Mg II is the only strong line present until C III enters at $z \approx 1.0$. Other features are the dips at $z \approx 1.9$ and $z \approx 2.6$, as first C III and then C IV pass through the strong sky line at 5577 Å, and the high detection probabilities from $z \approx 2$, when Ly α enters, up to $z \approx 3.5$, when C IV passes out of range and the detection probability again falls to zero.

This relation can be used to obtain a tighter upper limit on the QSO surface density. If we make the assumption that the number of QSOs per redshift interval does not decrease with redshift out to $z = 3.5$, then *regardless of the detailed shape of the redshift distribution* the minimum fraction of QSOs we would have identified (by the above criteria) is 38 per cent. Since we identify two QSOs, this suggests that the true number of QSOs in the survey is around five, a surface density of 160 deg^{-2}. At the upper 1 per cent confidence,

© Royal Astronomical Society • Provided by the NASA Astrophysics Data System

1991MNRAS.253..686C

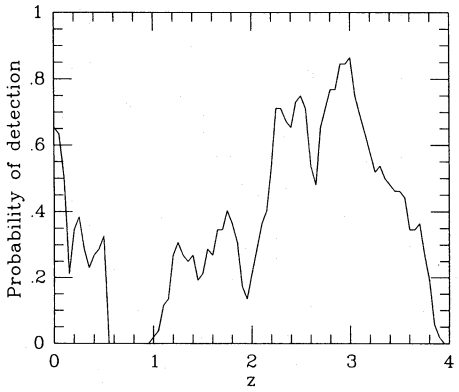

Figure 7. The detectability of a typical QSO in the unidentified spectra, as a function of redshift. The detectability at a given redshift is defined as the fraction of unidentified survey spectra in which the redshifted composite spectrum of Francis *et al.* (1991) would have at least one emission line with $S/N_{\rm line} > 6$ and at least one other confirming line with $S/N_{\rm line} > 4$.

however, Poisson statistics tell us that finding two QSOs is consistent with finding eight, giving us a 1 per cent confidence level upper limit of 21 for the true number of QSOs in the survey. This corresponds to a surface density of 550 deg^{-2} for QSOs with $z < 3.5$ in the magnitude range $21 \leqslant b_J \leqslant 23.5$, less than half the value obtained by crudely assuming that all unidentified objects were QSOs.

If we relax our assumption that the number of QSOs per redshift interval does not decrease, then our estimate of the true number of QSOs in the survey will depend explicitly on our model for the redshift distribution. However the model-independent estimate given above should remain a good approximation due to the fact that plausible models only predict a significant decrease in the number of QSOs per redshift interval for $z > 2$, where our probability of detection is high. For example, in a model where the QSO luminosity function evolves as $(1+z)^{3.5}$ up to $z = 2$ and the space density of QSOs is constant for $z > 2$ (Boyle, private communication), we find that we expect to identify 35 per cent of the QSOs in the sample despite the fact that the number of QSOs per redshift interval is falling fairly steeply for $z > 2$.

A compilation of previous number counts of $z < 3.3$ QSOs in the B-band by Hartwick & Schade (1990) is shown in Fig. 8, along with the number–magnitude relations for QSOs predicted by two simple models. The first of these models, due to Braccesi *et al.* (1980), assumes pure density evolution (PDE) for the QSO luminosity function and can be represented by $\log[n(B)] = 0.864(B - 18.31)$, where $n(B)$ is the surface density per square degree in a 0.5 mag bin centred on B. Such a power law fits the observations brighter than $B \approx 20$ adequately, but the fainter results suggest a flattening in count slope. Even our strict upper limit, which crudely assumes all the unidentified objects are QSOs, lies more than a factor of 20 below the value that would be predicted from an extrapolation of the Braccesi *et al.* (1980) relation. This apparent turnover led Boyle *et al.* (1987) to propose a pure luminosity evolution (PLE) model (for $z < 2.2$ QSOs) which better fits the data.

In order to compare our LDSS QSO count with earlier data, we assume that the faint end of $n(B)$ is adequately approximated by a power law, which we normalize by noting

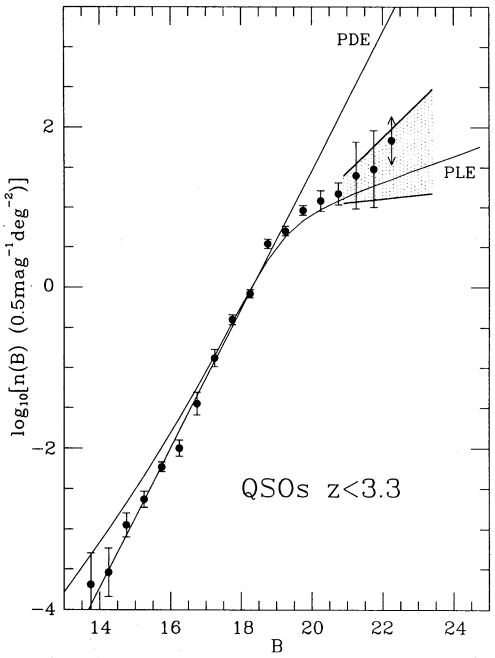

Figure 8. The differential number–magnitude relation for QSOs with $z < 3.3$. The points with error bars are taken from the compilation of QSO number counts by Hartwick & Schade (1990). The faintest point comes from the counts of Koo *et al.* (1986) and Koo & Kron (1988), for which the Poisson errors shown may underestimate the true errors. The range between the upper and lower limits on the QSO number–magnitude relation obtained from this survey is shown as the shaded region. The line labelled PDE indicates the Braccesi *et al.* (1980) power-law relation. The line labelled PLE indicates the pure luminosity evolution model of Boyle *et al.* (1987) for $z < 2.2$ QSOs.

that $n(B) \approx 10$ at $B = 20$, the point at which the counts first appear to deviate from the power law that fits the observations at brighter magnitudes (see Fig. 8). With this normalization, a self-consistent value for the power-law slope for $B > 20$ follows directly from the surface density of QSOs in the magnitude interval covered by our survey ($20.9 \leqslant B \leqslant 23.4$, where we have transformed to B magnitudes using $B = b_J - 0.1$ for QSOs in accord with Boyle (1986)). The lower limit on the slope of the number–magnitude relation obtained in this fashion from the two QSOs unambiguously identified in the survey is 0.05. The 1 per cent confidence upper limit, derived from our estimate of the detectability of QSOs in the survey, gives a slope of 0.43. The permitted range of the QSO number–magnitude relation corresponding to these limits is indicated in Fig. 8 by the shaded region. As an absolute upper limit, the assumption that all unidentified objects in the survey are QSOs gives a slope of 0.55. These limits on the number–magnitude relation of faint QSOs are especially significant since (i) they are obtained from a sample of compact objects without selection by colour or any other property, and (ii) in fact they apply to QSOs with redshifts up to $z = 3.5$, and not just $z < 2.2$.

The most directly comparable results are those of Koo *et al.* (1986) and Koo & Kron (1988). The faintest point shown in Fig. 8 indicates the surface densities of QSOs corresponding to the number of objects listed in table 1 of Koo & Kron as probable QSOs based on spectroscopic, colour and variability criteria (summary object type 'B'). Only Poisson error

© Royal Astronomical Society • Provided by the NASA Astrophysics Data System

1991MNRAS.253..686C

bars are shown. The power-law slope computed from the Koo & Kron data is 0.38 ± 0.06, consistent within the errors with the value of 0.31 ± 0.05 obtained by Boyle, Shanks & Peterson (1988) for $z < 2.2$ QSOs, and falling slightly below the upper limit for the slope of 0.43 obtained here.

The results of this survey strongly support and extend the suggestion by Koo *et al.* (1986) and Boyle *et al.* (1987) that the number–magnitude relation for QSOs turns over around $B = 20$. Whilst our sample is small, we calculate that our spectra have sufficient signal to noise to reveal QSO features across the entire redshift range expected. Provided QSOs have, on average, spectra similar to that of the Francis *et al.* (1991) composite, we can place a strong upper limit on the number of faint QSOs whose detectability depends solely on their line properties. Together with earlier data, this result confirms that the QSO number–magnitude relation flattens at faint limits, and that the surface density of QSOs per square degree per 0.5 mag interval is consistent with a power-law slope in the range 0.05 to 0.43. This result rules out the pure density evolution model for QSOs proposed by Braccesi *et al.* (1980), but is consistent with the colour-selected QSO counts of Koo & Kron (1988) and the pure luminosity evolution model suggested by Boyle *et al.* (1987).

6 THE DISTRIBUTION OF FAINT STARS

A bimodal colour distribution for faint stars (to $B \sim 23$) was recognized many years ago (e.g. Kron 1980; see also Fig. 6a) as arising from the different distances probed for stars of spectral types G through M. The first quantitative multipass-band analysis of faint ($B > 20$) stars in terms of Galactic structure was that of Gilmore & Reid (1983). From photometric distances (assuming a population I main-sequence luminosity scale) of stars to $B \approx 21$–22 at the South Galactic pole, they claimed the density profile at distances of 2–4 kpc indicated a much larger scaleheight ($H \approx 1.3$ kpc) than a simple two-component ('thin' $H \approx 0.3$ kpc disc and spheroid) model could reproduce. They postulated the existence of a new intermediate-age 'thick disc' Galactic component whose presence may indicate recent star formation and/or dynamical activity in the Galaxy. Dynamical and compositional investigations of large numbers of selected brighter stars support this conjecture (see review by Gilmore, Wyse & Kuijken 1989).

A major goal of Tritton & Morton's (1984) survey was to constrain the properties and abundances of stars at large distances from the Sun. Although their spectroscopic sample of ~ 600 stars is considerably smaller than Gilmore & Reid's purely photometric analysis of 12 500 stars, it supported the existence of a thick disc with analysis in a new direction and using a more rigorously defined data set. Tritton & Morton derived a scaleheight of $H \approx 0.7 \pm 0.1$ kpc.

Our two spectral surveys (this paper and Paper I) jointly contain colours for a sample of 91 spectroscopically confirmed stars, some at very large distances from the thin disc. The $b_J = 23.5$ limit corresponds to distances of 1–10 kpc for red main-sequence stars (spectral types M5V through K5V), and of course considerably greater distances if contamination by subgiants is considered important. It is therefore of interest to compare the numbers of faint stars found with the predictions of the proposed two- and three-component models of the Galaxy for the two directions we have studied.

In making such comparisons, the most important feature of the sample of stars in this survey is that they are not only faint but also spectroscopically confirmed. Thus, at least where we have a reasonably high identification rate, we have isolated the stellar population from the very much larger galaxy population that dominates the overall numbers at such faint magnitudes. As Gilmore *et al.* (1989) note in their review of star count data, fainter than $V = 21$ the precision of star counts becomes dominated by the large numbers of galaxies contaminating the samples due to systematic errors in the star–galaxy separation. Our sample thus provides the only window on the colour–magnitude distribution for stars fainter than $V = 21$ that does not suffer overwhelmingly from this problem. The estimated 16 per cent incompleteness for stars, resulting from uncertainties in image classifications (see Section 2), is not significant at the level at which we can make comparisons, since the small size of the sample (91 confirmed stars with $21 \leqslant b_J \leqslant 23.5$) means that only gross variations in the colour–magnitude relation will be detectable.

Additionally, this magnitude range is particularly suitable for examining the thick disc component of the Galactic stellar population, since only fainter than $B = 21$ do the intermediate population II stars become a major component of the total stellar population. This can be seen in Fig. 9, which shows the $b_J - r_F$ versus b_J colour–magnitude distributions predicted in each of the two survey fields in Galactic structure models with and without a thick disc component. These models were generated using the GALAXY program of G. Gilmore (private communication), and have the parameters given in Table 4. The three-component model including an intermediate population II thick disc is very close to that originally suggested by Gilmore & Reid (1983). The two-component model is the same as the three-component model save for the lack of a thick disc.

As Fig. 9 shows, the colur–magnitude distribution of stars with $21 \leqslant b_J \leqslant 23.5$ has the classical bimodal colour distribution, with peaks at $b_J - r_F \approx 2.5$ and $b_J - r_F \approx 0.7$, but with a third peak (or shoulder, depending on the field) at $b_J - r_F \approx 2.0$. The difference made by adding the intermediate population II thick disc stars is the enhancement of this third peak in the colour distribution by a factor of 3 or more over the two-component model. In the 10-hr survey field (at $l = 248°$, $b = 49°$) this peak becomes stronger than the blue peak and about two-thirds as strong as the red peak, while in the 13-hr field (at $l = 330°$, $b = 60°$) it is clearly dominant. Because this peak lies at $b_J - r_F \approx 2.0$, where our success rate for identifications is high (~ 80 per cent), we therefore can use our spectroscopic survey to test for the existence of the thick disc in a magnitude regime that has not previously been accessible to observation. Alternatively (given that there is considerable evidence for the existence of the thick disc at brighter magnitudes), this might be restated as testing the faint end of the intermediate population II luminosity function.

As with the QSOs discussed in the previous section, the true number of stars in our survey must lie somewhere between the number identified spectroscopically as stars (hereafter STARS) and the number of objects that are *not* spectroscopically confirmed to be galaxies or QSOs (hereafter NONGAL). The colour–magnitude distributions for these two classes are shown in Fig. 10, and provide lower

© Royal Astronomical Society • Provided by the NASA Astrophysics Data System

1991MNRAS.253..686C

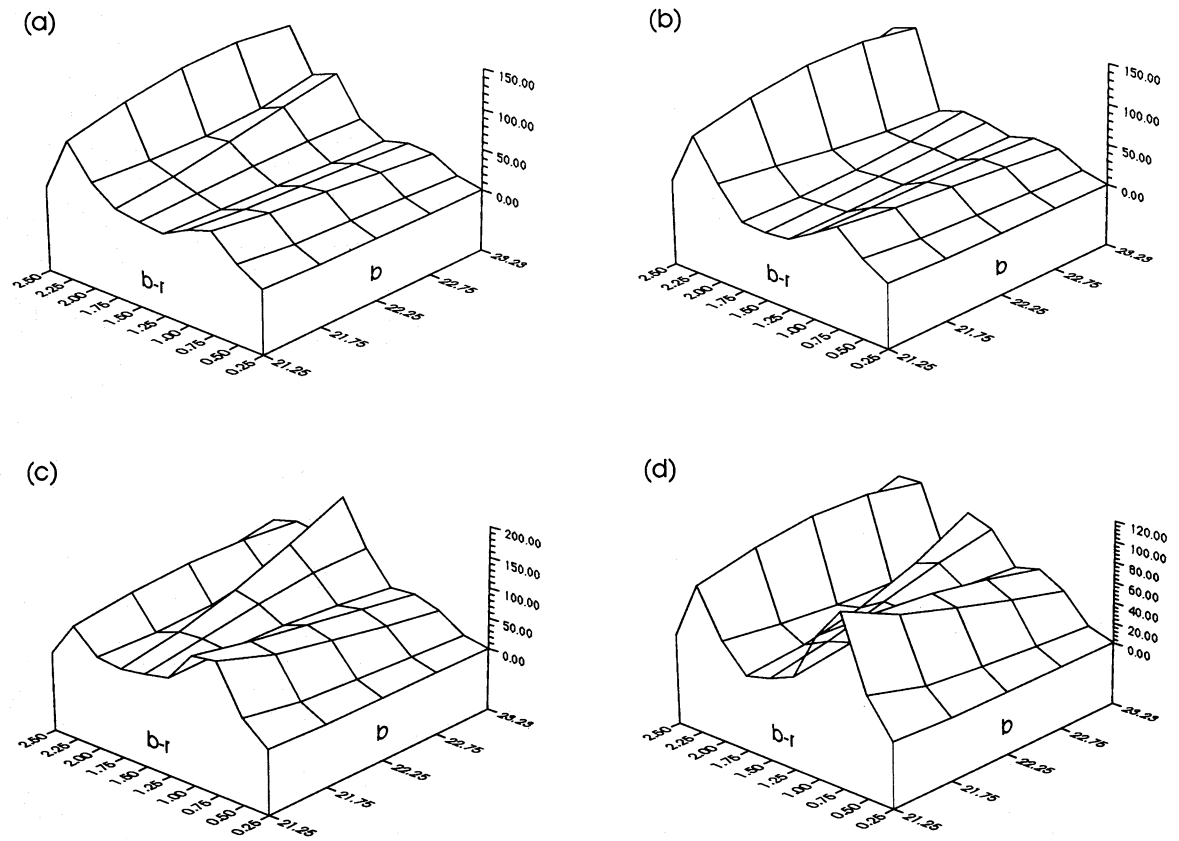

Figure 9. Model stellar $b_J - r_F$ versus b_J distributions: (a) 10-hr field, thick disc; (b) 10-hr field, no thick disc; (c) 13-hr field, thick disc; (d) 13-hr field, no thick disc. Table 4 gives model details.

Table 4. Parameters of Galactic structure models.

Components of the model:
1. a Population I old disk (PI)
2. an intermediate Population II thick disk (IPII)
3. an extreme Population II spheroid (EPII)

General parameters:
1. the solar distance from galactic centre is 8000 pc
2. local extinction is 0.00 mag distributed above the plane with a scale height of 100 pc and radially in the plane with constant density

Disk structural parameters:
1. the PI luminosity function is that due to Wielen/Gilmore
2. the radial exponential scale length is 3500 pc cut off at 5 scale lengths
3. the main sequence perpendicular scale height is 325 pc
4. the disk red giant perpendicular scale height is 250 pc
5. the white dwarf perpendicular scale height is 250 pc

Spheroid structural parameters:
1. the EPII and IPII luminosity function is the Weilen function for $M_V > +4.5$, and the da Costa 47 Tuc function for $M_V < +4.5$, with a hb:rg ratio of 5 for $0.5 < M_V < 1.0$
2. the c-m relation for the IPII is that of 47 Tuc
3. the local IPII:PI number ratio is 0.02
4. the thick disk density law is an exponential with scale height 1300 pc and scale length 3500 pc in the galactic plane
5. the c-m relation of the outer spheroid is that of M5
6. the local EPII:PI stellar number ratio is 0.00125
7. the spheroid density law is a deVaucouleurs spheroid with Re=2700 pc and minor/major axis ratio 0.80

and upper bounds (at least within the Poisson errors) on the true colour–magnitude distribution of stars. The STARS and NONGAL distributions for both fields are given in Table 5 as numbers per square degree, and are computed using the sampling rates given in Section 2 and the field areas given in Table 2 for the stars from this survey and those given in Paper I for the high-dispersion survey. Two features of the observed distributions are immediately apparent: (i) because of the small numbers involved, the distributions are very noisy; and (ii) the significant contamination of the sample by galaxies is apparent as the large number of unidentified objects with blue colours showing up in the NONGAL distribution.

One-sample χ^2-tests comparing the observed distributions to the models of Fig. 9 show that the contaminating galaxies make the NONGAL distribution significantly different to either model, but that the STARS distribution is consistent with both. Of course the poor success rate for identifications in the blue and the large number of bins in the distribution which have low expectation values mean that this is a very weak test for distinguishing the models. As noted above, a much more stringent test can be obtained by confining the comparison to the colour range $1.5 \leqslant b_J - r_F \leqslant 2.5$, which straddles the peak in the colour distribution that is so strongly enhanced in the presence of the thick disc. By limiting the colour range in this manner we have not only highlighted the difference between the two models, but also eliminated the blue contaminating galaxies and increased the effective success rate for identifications to 81 per cent. This has the result of bringing the NONGAL and STARS distributions closer together, as is evidenced in Table 6 by the very similar significance levels for the STARS and NONGAL distributions returned by one-sample χ^2-tests over this limited colour range. In both the 10- and 13-hr fields the thick disc model is an acceptable fit to the data, and is a

© Royal Astronomical Society • Provided by the NASA Astrophysics Data System

1991MNRAS.253..686C

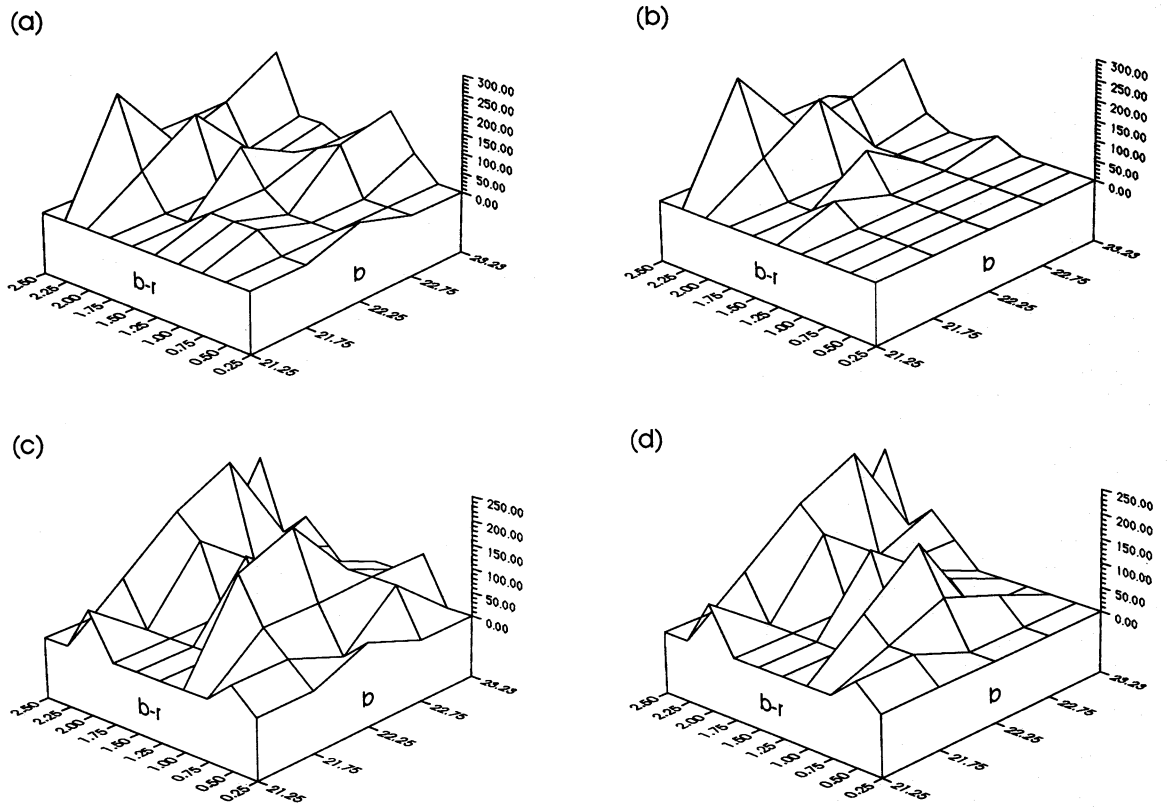

Figure 10. Observed $b_J - r_F$ versus b_J distributions: (a)10-hr field, NONGAL; (b) 10-hr field, STARS; (c) 13-hr field, NONGAL; (d) 13-hr field, STARS. (STARS means spectroscopically confirmed stars, NONGAL means objects not identified as galaxies or QSOs).

Table 5. Surface densities (deg^{-2}) of spectroscopically confirmed stars (STARS) and objects not identified as galaxies (NONGAL).

(a) 10hr field STARS:

	$b_J - r_F$										
b_J	0.25	0.50	0.75	1.00	1.25	1.50	1.75	2.00	2.25	2.50	Total
21.25	0	0	0	0	0	0	0	0	0	0	0
21.75	0	0	0	0	44	0	0	89	266	0	399
22.25	0	0	0	0	0	89	0	177	89	89	444
22.75	0	0	0	0	0	0	0	0	105	91	196
23.25	0	0	0	0	30	0	0	30	152	30	242
Total	0	0	0	0	74	89	0	296	612	210	1281

(b) 10hr field NONGAL:

	$b_J - r_F$										
b_J	0.25	0.50	0.75	1.00	1.25	1.50	1.75	2.00	2.25	2.50	Total
21.25	0	0	0	0	0	0	0	0	0	0	0
21.75	0	0	44	44	44	0	0	89	266	0	487
22.25	44	0	0	0	44	133	0	177	89	89	576
22.75	0	0	0	121	91	61	30	30	135	91	559
23.25	0	0	61	152	91	30	61	61	212	61	729
Total	44	0	105	317	270	224	91	357	702	241	2351

(c) 13hr field STARS:

	$b_J - r_F$										
b_J	0.25	0.50	0.75	1.00	1.25	1.50	1.75	2.00	2.25	2.50	Total
21.25	0	46	0	0	0	0	0	93	0	0	139
21.75	0	46	46	93	0	0	0	0	93	0	278
22.25	0	0	93	185	0	139	0	139	185	0	741
22.75	0	0	49	0	49	49	49	49	245	0	490
23.25	0	0	0	0	0	0	49	98	49	196	392
Total	0	92	188	278	49	188	98	379	572	196	2040

(d) 13hr field NONGAL:

	$b_J - r_F$										
b_J	0.25	0.50	0.75	1.00	1.25	1.50	1.75	2.00	2.25	2.50	Total
21.25	0	46	0	0	0	0	0	93	0	0	139
21.75	0	46	93	185	0	0	0	0	93	0	417
22.25	46	0	93	232	0	139	0	139	185	0	834
22.75	0	98	98	98	98	49	98	49	245	0	833
23.25	0	0	98	49	49	0	49	98	49	196	588
Total	46	190	382	564	147	188	147	379	572	196	2811

better fit than the model lacking a thick disc. The two-component model provides an acceptable fit to the data in the 13-hr field, but yields a very poor fit (to both the STARS and NONGAL distributions) in the 10-hr field.

The current sample is clearly too small to establish the parameters of the thick disc, but it does provide evidence for the existence at apparent magnitudes up to $b_J = 23.5$ of a thick disc consistent with that originally suggested by Gilmore & Reid (1983) from observations of stars two magnitudes brighter. The conclusion from this survey that at least 80 per cent of all compact objects redder than $b_J - r_F = 1.8$ are stars also implies that tests of Galactic structure using counts of red-selected stellar objects at these faint magnitudes will not suffer systematic errors greater than 10 per cent due to contamination by non-stellar objects. In the following section we use this observation to derive new upper limits on the numbers of red compact extragalactic objects.

7 LIMITS ON COMPACT EXTRAGALACTIC OBJECTS

Distant galaxies are rendered faint by several cosmological processes, of which the combined effect of the relativistic distance modulus and K-correction is the most reliably modelled. A less well-understood effect is surface brightness dimming, which has a strong redshift dependence [$\propto (1+z)^4$], and which could introduce important biases in the population of distant objects selected in faint surveys (*cf.* Disney & Phillipps 1983; Davies 1990). For example, King

© Royal Astronomical Society • Provided by the NASA Astrophysics Data System

1991MNRAS.253..686C

Table 6. Significance levels from χ^2-test comparisons with models of the Galaxy with and without a thick disc.

	10hr field		13hr field	
	STARS	NONGAL	STARS	NONGAL
Thick disk	0.07	0.17	0.19	0.23
No thick disk	0.01	<0.001	0.05	0.05

& Ellis (1985) postulated that for certain cosmological and evolutionary models a two-component bulge + disc galaxy might be recognized only as a compact object. In principle a number of very faint compact sources might be cosmologically interesting objects. Interestingly, spectroscopic surveys of very faint *extended* objects (to $b_J \approx 23$–24) fail to find any significant high-redshift population (Lilly, Cowie & Gardner 1991; Colless *et al.*, in preparation) yet the surface density of very faint sources implies extraordinarily large volumes are being sampled. One possible solution to this dilemma might be the existence of a population of compact objects which is relatively rare in the interval $22.5 < b_J < 24$ but which rises in number rapidly to fainter apparent magnitudes (because of evolutionary effects), such that it is a major contributor to the perplexing abundance of all objects at $b_J \approx 26$–27 (where star/galaxy separation is not attempted).

An additional motivation for searching for extragalactic objects that remain rare at $b_J \approx 23$ but become important at fainter magnitudes, is to constrain the volume density of *local* objects (i.e. objects so intrinsically faint that they will not be detected at cosmological distances). Such a local population would have a number–magnitude relation with Euclidean slope [$d \log n(m)/dm = 0.6$], and so its number would also increase with apparent magnitude much faster than is the case for normal galaxies [which are observed to have $d \log n(m)/dm \approx 0.45$]. Interestingly, the recognized extragalactic objects (other than QSOs) in our survey appear to fall into two categories. Of seven galaxies (*cf.* Fig. 4), four have $z \approx 0.3$–0.4 in reasonable agreement with other galaxy surveys at brighter or comparable limits – i.e. they are consistent with misclassification of normal faint galaxies. However, at least one (10.2.11) and possibly a further two (10.2.27 and 10.4.09) are very low-luminosity systems. For example, 10.2.11 has $z = 0.030$ and an absolute magnitude of only $M_{b_J} = 12.1 + 5 \log h$. Proper constraints on the numbers of such dwarf galaxies outside clustered fields would be valuable.

The incompleteness of this survey as a function of colour is a major obstacle to a proper analysis of this question. However we can place useful limits on those populations of compact extragalactic objects whose colours lie at the extremities of our $b_J - r_F$ distribution, where our completeness is moderately good.

The procedure we have adopted is to derive an upper limit to the surface density of those compact objects whose spectroscopic identity is unknown (hereafter 'unknowns'), as a function of colour, from both the current survey ($21 \leqslant b_J \leqslant 23.5$) and that of Paper I ($21 \leqslant b_J \leqslant 22.5$). We ignore objects from Paper I classified as extended by COSMOS for which no spectroscopic identification was achieved because, despite possible classification errors in individual cases, the COSMOS separation was, on the whole, statistically reliable. Allowing for the sampling rate of the surveys in the two magnitude intervals, we obtain the surface density of 'unknowns' as a function of colour (Table 7). The 'unknowns'

Table 7. Colour distribution of unknown compact sources.

	Number (deg^{-2})	
$b_J - r_F$	$21 \leq b_J \leq 22.5$	$22.5 \leq b_J \leq 23.5$
<0.25	—	—
0.25–0.50	71	19
0.50–0.75	82	56
0.75–1.00	94	150
1.00–1.25	82	224
1.25–1.50	118	37
1.50–1.75	—	56
1.75–2.00	—	56
2.00–2.25	35	56
2.25–2.50	—	56
2.50–2.75	—	38
2.75–3.00	—	19
>3.00	—	—
No colour	71	94
Total unknown	552	804
Total compact	1333	1560
All objects	5620	10427

in the $21 \leqslant b_J \leqslant 22.5$ interval represent 41 per cent of all compacts and 10 per cent of all objects for the three survey fields. For the fainter $22.5 \leqslant b_J \leqslant 23.5$ interval, the figures are 51 and 8 per cent respectively. Given the poor signal/noise ratio of much of the fainter data, it is important to realize that these numbers represent an *upper limit* to any possible new population of objects, particularly at intermediate colours where unrecognized absorption-line galaxies are likely to be common.

If we assume the 'unknowns' represent one or more new populations sharing a Euclidean $d \log n(m)/dm = 0.6$ slope, we can ask what is the *maximum* contribution an 'unknown' of any colour might make to the very faint ($B > 26$) galaxy counts. This is the most straightforward way of asking whether there is any evidence in the LDSS surveys for a significant new population. In practice the 'unknowns' from the fainter LDSS survey provide more useful constraints and we concentrate on those estimates in the following discussion. Although a Euclidean slope need not necessarily imply any such population is local, this is the simplest approximation given we can make no assumptions about the redshifts or spectral energy distributions of any hitherto undiscovered populations.

The faintest reliable colour distribution approximating our photographic filter system is that published by Guhathakurta, Tyson & Majewski (1990) which selects objects in the range $26 < b_J < 27$. Guhathakurta (private communication) claims an additional 25 per cent of objects found in this b_J range have no colours because they were fainter than the R detection limit of $R = 27.5$, implying that their colours are at least as blue as $b_J - R = -0.5$. We have therefore added this missing component to the colour distribution assuming those sources have $b_J - R < -0.5$. The resulting data, together with the projected (maximum contribution) colour distribution of 'unknowns' scaled from Table 7 to the fainter limits according to the Euclidean count slope and suitably normalized for the sky areas involved, is shown in Fig. 11.

Very significantly, half the deep data contains sources whose colours, $b_J - R < 0.25$, are outside the range sampled in the LDSS survey. If this faint blue population is represented at brighter magnitudes, its counterpart can only be in the galaxy category, there being insufficient blue compacts by an enormous factor. The maximum contribution compact objects could make to this population would arise if we

© Royal Astronomical Society • Provided by the NASA Astrophysics Data System

1991MNRAS.253..686C

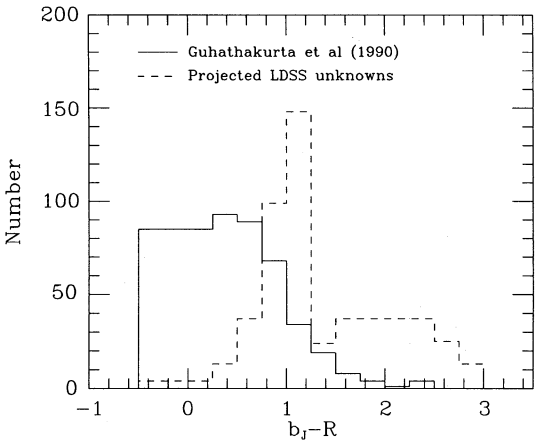

Figure 11. Observed $b_J - R$ colour distribution (solid line) for a sample of faint sources with $26 < b_J < 27$ (after Guhathakurta *et al.* 1990). The dashed histogram represents the maximum likely contamination by those compact sources classed as unknowns in the new LDSS survey (see text for details). Counts are for Guhathakurta *et al.*'s CCD field of view (18.9 arcmin^2).

assume that all LDSS sources without r_F detections are bluer than $b_J - r_F < 0.25$. Even then, the projected population of blue LDSS 'unknowns' fails to match the blue population at $b_J \approx 26$–27 by over an order of magnitude. Only two possibilities remain. *Either* the onset of blue compacts is remarkably rapid (i.e. there are effectively *no* brighter counterparts at $b_J \approx 23$), in which case the absence of a sudden upturn in the total counts over $24 < b_J < 27$ is surprising (Ellis 1990); *or* the blue objects at $b_J \approx 26$–27 are simply an extension of the well-studied galaxy population surveyed in Paper I.

Interestingly, those *known* sources at the blue end of the colour distribution of LDSS compacts are almost all QSOs and emission line galaxies. The former category was ruled out as a major component of the faint counts in Section 5, but emission line galaxies are a very likely contributor, especially if some proportion have low luminosity. The Guhathakurta *et al.* population most likely originates via a galaxy population which is represented at $b_J < 23$, but with some rarity and without perhaps the extreme colours. A relatively local ($z < 1$) starburst population, examples of which are found in both compact and extended object categories at these limits, may increase in significance (via the intensity and/or frequency of star formation activity) with look-back time. The effect this might have on the faint counts has been modelled by Broadhurst *et al.* (1988) and will be discussed further in a separate paper covering a recently completed survey of very faint blue sources without morphological selection (Colless *et al.*, in preparation).

At the *red* end of the colour distribution, we find the opposite effect. Our incomplete LDSS survey permits a modest population of red unknowns with $b_J - r_F > 1.5$ amongst a large population of cool Galactic stars, but almost no equivalently red sources are seen by Guhathakurta *et al.* Since any localized red populations (e.g. intergalactic globular clusters and red dwarf galaxies) would have Euclidean count slopes, their space density can be usefully constrained by the combination of the LDSS spectroscopy and the deep CCD data. For example, an old stellar system with, say, $M_B \approx -8 + 5 \log h$ would be visible to $\sim 100\ h^{-1}$ Mpc at the CCD limit of Guthakurta *et al.*, yet only about 10 per cent of the red LDSS 'unknowns' (and 2 per cent of all compacts to $b_J = 23.5$) are consistent with such a population. In the case of dwarf elliptical galaxies, whose current luminosity functions remain uncertain fainter than $M_B \approx -14$ (Binggeli, Sandage & Tammann 1988), significantly larger depths ($\sim 1000\ h^{-1}$ Mpc and upwards) are probed to $b_J \approx 26$–27, and consequently more secure upper limits on their number density can be provided.

Taking first the case of globular clusters, we will assume these objects follow a Gaussian luminosity function of width 2 mag centred at $M_B = -8$ (Harris & Racine 1979). The number of Guhathakurta *et al.*'s red objects (17 in their 18.9 arcmin^2 CCD field) yields an upper limit of $23 \pm 5\ h^{-3}$ Mpc^{-3} for the space density of such objects. However, to $b_J = 23.5$, the LDSS survey indicates that the bulk of the red compacts are Galactic M stars, whose spectral features are readily distinguishable from globular clusters. Depending on the number–magnitude relation for Galactic stars in the interval $23 < b_J < 27$, a fraction of the faint red population will be M stars, and thus the space density above is an overestimate. We can make a rough estimate of the fraction of contributing stars at $b_J \approx 27$ if we assume the thick disc model described in Section 6. Using Gilmore's GALAXY program and normalizing its prediction with the actual number of M stars found in our survey between $21 \leqslant b_J \leqslant 23.5$, of the 17 red objects in Guhathakurta *et al.*'s data, 10 could be Galactic stars. Thus the spatial density of isolated extragalactic globular clusters could be as low as $10\ h^{-3}$ Mpc^{-3}. This is an interesting limit considering the volume density associated with luminous galaxies is $\sim 2000 \times \phi^* \approx 30\ h^{-3}$ Mpc^{-3}. We note that the absence of very faint globular clusters is not in conflict with the high abundance of such systems seen around luminous galaxies because the Guhathakurta *et al.* field is very unlikely to contain even one L* field galaxy closer than $100\ h^{-1}$ Mpc.

For the dwarf ellipticals (dEs) similar arguments apply. Binggeli *et al.* (1988) have already suggested the field dE luminosity function must be considerably flatter at the faint end than that measured in the Virgo cluster. Adopting their tentative field luminosity function with $\alpha = -1.0$, we would expect ~ 40 dEs in the Guhathakurta *et al.* field. Were the luminosity function as steep as in the Virgo cluster ($\alpha = -1.35$), the prediction would increase by at least 25 per cent (depending on the faint end cut-off). There is in fact a slight conflict, since the upper limit on observed number of dEs is only 17. Clearly, there is no significant population of intrinsically faint dEs.

Thus, in conclusion, the bulk of the very faint sources found in the deep CCD surveys must be galaxies, and by implication, the noticeable colour shift must represent the bulk evolution of some subset of the galaxy population. The rapid decline of the red population with increasing magnitude signals the edge of the Galaxy and a marked paucity in any extragalactic red population of low-luminosity objects.

8 CONCLUSIONS

We have obtained low-resolution spectra for 117 compact objects with $21 \leqslant b_J \leqslant 23.5$. The survey sample was selected only by apparent magnitude and an image compactness criterion. By choosing compact objects we have been able to reach a limit one magnitude fainter than our previous all-

© Royal Astronomical Society • Provided by the NASA Astrophysics Data System

1991MNRAS.253..686C

object survey (Colless *et al.* 1990), while achieving a success rate for spectroscopic identifications of 57 per cent. The prime motivation for this survey was to place limits on the numbers of faint stars, QSOs and any other population of objects (perhaps hitherto undiscovered) with near-stellar images. Of the 67 identified objects, 58 are stars, seven galaxies and two QSOs. Because the completeness of the spectroscopic identifications in the survey is a strong function of colour, with success rates of 70 per cent for the bluest objects and 90 per cent for the reddest, we are able to derive strong constraints on several interesting types of object with extreme colours.

(1) From the two QSOs identified in the survey we obtain a lower limit on the surface density of QSOs with $21 \leqslant b_J \leqslant 23.5$ of 64 deg^{-1}. Using the criteria by which these two objects were identified, we estimate, as a function of redshift for each of the unidentified spectra in the survey, the probability of detecting a 'typical' QSO [represented by the composite spectrum of Francis *et al.* (1991)]. Assuming only that the redshift distribution of QSOs does not decrease with redshift out to $z = 3.5$, we find that we should have identified *at least* 38 per cent of 'typical' QSOs. This implies a 1 per cent confidence level upper limit to the surface density in the interval $21 \leqslant b_J \leqslant 23.5$ of 550 deg^{-1}. Approximating the number of QSOs per square degree per 0.5 mag between $B = 20$ and 23.5 by a power law, these lower and upper limits correspond to slopes, $d \log n(m)/dm$, of 0.05 and 0.43 respectively. These results confirm and extend the suggestion by Koo *et al.* (1986) and Boyle *et al.* (1987) that the number–magnitude relation for QSOs turns over around $B \approx 20$, with $d \log n(m)/dm$ changing from 0.86 at brighter magnitudes to a value less than 0.43 at fainter magnitudes. This confirmation is especially significant since the sample is selected only by magnitude and image compactness, and thus is more inclusive than previous studies which have employed additional selection criteria such as colour or variability.

(2) Combining this survey with the brighter survey of Colless *et al.* (1990) gives magnitudes and colours for a sample of 91 spectroscopically confirmed stars between $b_J = 21$ and 23.5. The faint limit corresponds to distances of 1–10 kpc for spectral types M5V through K5V, so that we are able to test the predictions of Galactic structure models for common main-sequence stars at relatively large distances. While this sample is too small to strongly constrain the structural parameters of the models, it does provide support for the existence in this regime of a thick disc consistent with that originally suggested by Gilmore & Reid (1983) from observations at brighter magnitude limits.

(3) More generally, we derive upper limits as a function of colour on the surface density of spectroscopically unidentified objects in the range $21 \leqslant b_J \leqslant 23.5$. As noted above, the strong variation in the completeness of the survey with colour means that the most useful limits are obtained for classes of object with extreme colours. These limits are of particular interest when applied to classes of red and blue compact *extragalactic* objects in the context of a population with an assumed $d \log n(m)/dm$ of 0.6. Such a Euclidean number–magnitude relation is most straightforwardly interpreted as a faint local population, but could also represent the extreme case of a class of bright distant objects showing a rapid onset at faint apparent magnitudes. For such a population, an extrapolation to $b_J \approx 26$–27 of the numbers of unidentified *blue* compact objects we find at $b_J < 23.5$ shows a deficit of more than an order of magnitude compared to the actual surface density of all blue objects in this magnitude range found by Guhathakurta *et al.* (1990). This argues strongly that the faint blue population they observe is unrelated to any class of compact object present in the LDSS sample, and must be due to bulk trends in the galaxy population. Conversely, at the *red* end of the colour distribution our incompleteness permits a modest population of compact red objects in addition to a much larger population of Galactic stars. However at $b_J \approx 26$–27 Guhathakurta *et al.* find far fewer red sources than we would predict from a Euclidean extrapolation of our red unknowns. Thus the abundances of intrinsically faint populations of red compact objects must be exceedingly low. Intergalactic globular clusters with $M_B \approx -8$ would be detected by Guhathakurta *et al.* out to 100 h^{-1} Mpc, yielding an upper limit of $23 \pm 5\ h^{-3}$ Mpc^{-3} on their abundance. Similar arguments apply to dwarf elliptical (dE) galaxies, whose luminosity function cannot have a faint end slope as steep as that observed in the Virgo cluster by Binggeli *et al.* (1988).

ACKNOWLEDGMENTS

We acknowledge the generous allocations of time on the Anglo-Australian Telescope which made this work possible. The photographic photometry was performed on the COSMOS machine at the Royal Observatory, Edinburgh, and calibrated with CCD data kindly supplied by Laurence Jones and by Karl Glazebrook, Lance Miller and Chris Collins. We thank Raja Guhathakurta for supplying data in machine-readable form. The computing and data reduction was carried out on STARLINK, which is funded by the SERC. MMC acknowledges the support of a SERC PDRA and a Fellowship at King's College, Cambridge. RSE and GDS acknowledge financial support from SERC.

REFERENCES

Binggeli, B., Sandage, A. & Tammann, G. A., 1988. *Ann. Rev. Astr. Astrophys.*, **26,** 509.
Boyle, B., 1986. *PhD thesis*, University of Durham.
Boyle, B. J., Shanks, T. & Peterson, B. A., 1988. *Mon. Not. R. astr. Soc.*, **235,** 935.
Boyle, B. J., Shanks, T., Fong, R. & Peterson, B. A., 1987. *Mon. Not. R. astr. Soc.*, **227,** 717.
Braccesi, A., Zitelli, V., Bonoli, F. & Formiggini, L., 1980. *Astr. Astrophys.*, **85,** 80.
Broadhurst, T. J., Ellis, R. S. & Shanks, T., 1988. *Mon. Not. R. astr. Soc.*, **235,** 827.
Colless, M. M., Ellis, R. S., Taylor, K. & Hook, R. N., 1990. *Mon. Not. R. astr. Soc.*, **244,** 408 (Paper I).
Davies, J. I., 1990. *Mon. Not. R. astr. Soc.*, **244,** 8.
Disney, M. & Phillipps, S., 1983. *Mon. Not. R. astr. Soc.*, **205,** 1253.
Ellis, R. S., 1990. In: *Hubble Centennial Symposium*, ed. Kron, R., p. 248, ASP Conference Series, San Francisco.
Ellis, R. S. & Parry, I. R., 1988. In: *Instrumentation for Ground-Based Astronomy,* ed. Robinson, L., p. 192, Springer-Verlag, New York.
Francis, P. J., Hewettt, P. C., Foltz, C. B., Chaffee, F. H., Weymann, R. J. & Morris, S. L., 1991. *Astrophys. J.*, **373,** 465.
Gilmore, G. & Reid, N., 1983. *Mon. Not. R. astr. Soc.*, **202,** 1025.
Gilmore, G., Wyse, R. F. G. & Kuijken, K., 1989. *Ann. Rev. Astr. Astrophys.*, **27,** 555.

© Royal Astronomical Society • Provided by the NASA Astrophysics Data System

1991MNRAS.253..686C

Guhathakurta, P., Tyson, A. J. & Majewski, S. R., 1990. *Astrophys. J.*, **357,** L9.
Harris, W. E. & Racine, R., 1979. *Ann. Rev. Astr. Astrophys.*, **17,** 241.
Hartwick, F. D. A. & Schade, D., 1990. *Ann. Rev. Astr. Astrophys.*, **28,** 437.
Jacoby, G. H., Hunter, D. A. & Christian, C. A., 1984. *Astrophys. J. Suppl.*, **56,** 257.
Jones, L. R., Shanks, T., Fong, R., Ellis, R. S. & Peterson, B. A., 1991. *Mon. Not. R. astr. Soc.*, **249,** 481.
King, C. R. & Ellis, R. S., 1985. *Astrophys. J.*, **288,** 456.
Koo, D. C. & Kron, R. G., 1988. *Astrophys. J.*, **325,** 92.
Koo, D. C., Kron, R. G. & Cudworth, L. M., 1986. *Publs astr. Soc. Pacif.*, **98,** 285.
Kron, R. G., 1980. *Astrophys. J. Suppl.*, **43,** 305.
Lilly, S. J., Cowie, L. L. & Gardner, J. P., 1991. *Astrophys. J.*, **369,** 79.
Morton, D. C., Krug, P. A. & Tritton, K. P., 1985. *Mon. Not. R. astr. Soc.*, **212,** 325.
Oke, J. B., 1974. *Astrophys. J. Suppl.*, **27,** 21.
Tritton, K. P. & Morton, D. C., 1984. *Mon. Not. R. astr. Soc.*, **209,** 429.
Wynne, C. G. & Worswick, S. P., 1988. *The Observatory*, **108,** 161.

© Royal Astronomical Society • Provided by the NASA Astrophysics Data System